

Chapter 1

Clustering in Light Nuclei; from the Stable to the Exotic

Martin Freer

1.1 Clusters and Correlations in Context

The structure of nuclear matter is rich and varied. In one light the nucleus may behave like a liquid drop, with its shape and size corresponding to a balance between the long(ish) range attractive and short range repulsive behaviour of the nucleon-nucleon interaction and the charges of the constituent protons. This liquid drop displays collective properties such as vibrations where vibrational modes distort the nuclear surface; it can be encouraged to deform and then can be rotated—as the droplet spins it stretches which provides a mechanism for the determination of the equation-of-state of the fluid. At a critical angular momentum the droplet will fission. Similarly as the mass of a nucleus increases, typically so does the number of protons and hence the charge. The repulsive Coulomb energy should cause the nucleus to spontaneously fission when the number of protons is close to 100. However, it is at this point that another crucial feature contributes which allows nuclei to exist beyond that point—shell effects. Shell structure, which features for light and heavy nuclei alike, is associated with the quantal properties of the nucleus and marks a deviation from the constituent particles to a picture in which the particles are represented by standing waves. The associated quantum states are those of the nuclear shell model and give rise to a sequence of magic numbers which are associated with enhanced stability. A superposition of the macroscopic liquid drop and microscopic shell model-like behaviour is required to describe the stability of nuclei beyond the point at which the charged liquid drop should explode.

For light nuclei there is a similar interplay between the collective and single-particle nature, but here details of the nature of the interaction between the nucleons becomes increasingly important. Correlations become a dominant feature. The pairing interaction is evident in the nature of the drip-lines, which define the limits of stability on both the proton and neutron-rich side of the chart of nuclides (see

M. Freer (✉)

School of Physics and Astronomy, University of Birmingham, Birmingham, B15 2TT, UK
e-mail: M.Freer@bham.ac.uk

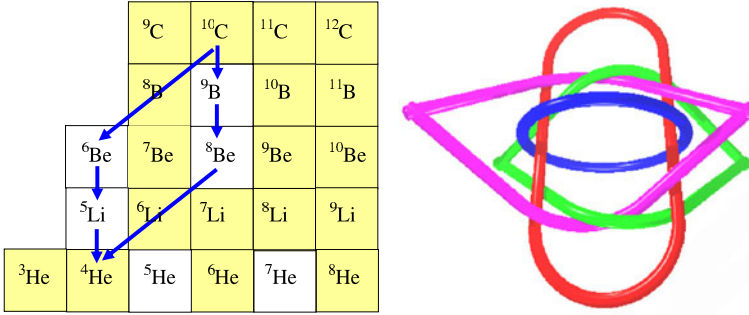


Fig. 1.1 Light nuclei. *Filled squares* are either stable or beta-decay, *unfilled particle* (neutron, proton or α) decay. The *arrows* show the paths corresponding to the removal of a proton or α -particle from ^{10}C . The diagram on the *right hand side* illustrates the 4th order Brunian knot

Fig. 1.1). For the helium nuclei, ^4He is stable, whereas ^5He is not. Similarly, ^6He and ^8He are stable and ^7He is not. The difference being that in addition to the ^4He core the stable isotopes have even numbers of neutrons, whereas the unstable ones do not. ^6He and ^8He are known as Borromean nuclei, as for example in the case of ^6He if a neutron is removed then the other two components dissociate; further if the α -particle is extracted then this leaves the unbound $2n$ system.

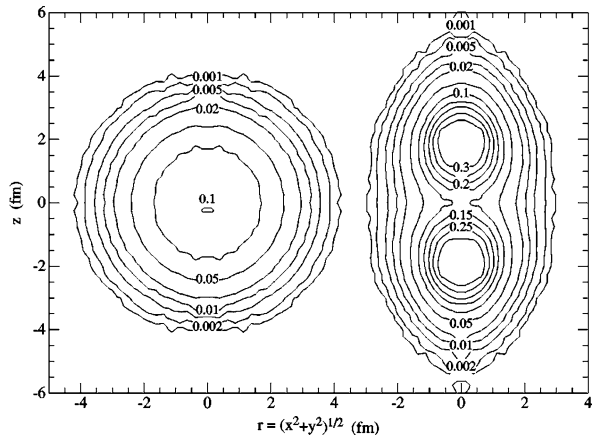
As an example of potentially exotic structures on the proton-rich side the ^{10}C nucleus sits at the head of a loop around unbound nuclei which include ^9B and ^8Be . ^{10}C may be thought of being composed of two protons and two α -particles and if any of the components are removed then the other three dissociate. This may be thought as a super-Borromean nucleus, or recognising that Borromean systems belong to a class of mathematical objects called Brunian knots then ^{10}C is a nucleus which is 4th order knot (as illustrated in Fig. 1.1).

These are rather extreme examples of correlations, but they are rather commonplace in light nuclei and have a determining role when it comes to the structure. These correlations can be spatial in addition to energy or momentum and then are referred to as clusters. The most prevalent cluster is the α -particle due to its remarkably high binding and inertness. This contribution examines some of the basic underlying principles behind the formation of clusters and examines some of the key areas experimentally where they strongly feature.

1.2 Clusters in First Principles Models

The formation of structures in nuclei that have large scale clustering is an intriguing phenomenon and is in part driven by correlations which stem from the details of the nucleon-nucleon interaction. For example, the *ab initio* Green's Function Monte Carlo (GFMC) calculations of ^8Be [1] predict the structure of nuclei based upon a starting point which is the nucleon-nucleon interaction expressed in terms of all two-body and three-body components. The two-body interactions are a parameterisation

Fig. 1.2 The Green's Function Monte Carlo calculations of the density of ${}^8\text{Be}$. The *left* and *right-hand* images are the densities calculated in the laboratory and intrinsic frames, respectively [1]. The 2α cluster structure is clearly evident



of the n - n force as determined from nucleon-nucleon scattering. It is not possible to determine the 3-body force in the same way, but is included through a parameterisation of terms such as the higher order pion exchange components devised by Fujita and Miyazawa [2]. In this manner the interaction is *ab initio* motivated rather than being grown from QCD. Given, that the model is one which contains the nucleonic degrees of freedom, it is somewhat remarkable that such an approach yields a ${}^8\text{Be}$ ground state, Fig. 1.2, that is clearly clustered [1]. At this point it is thus tempting to assert that the nucleus ${}^8\text{Be}$ corresponds to an α - α cluster structure in the ground state.

There have been many recent developments in the field of nuclear clusters including the ability to perform *ab initio* calculations of the light nuclei, such as the Green's Function Monte Carlo methods and Antisymmetrized Molecular Dynamics (Sect. 1.4.4) and Chiral Effective Field Theory (where nuclear properties are calculated on the lattice), the appearance of both experimental and theoretical evidence for molecular structures (Sect. 1.7) and the renewed focus on cluster states in nuclear synthesis, in particular the Hoyle-state in ${}^{12}\text{C}$ which may possess an α -condensate structure (Sect. 1.4.2). The following section attempts to provide a basic understanding of some of the underlying principles.

1.3 Appearance of the Nuclear Cluster from the Mean-Field

The possibility that the α -particles could be rearranged in some geometric fashion was realised even in the earliest days of the subject. An examination of the binding energy per nucleon of the light nuclei (Fig. 1.3—left-hand-side) shows that the nuclei which have even, and equal, number of protons and neutrons (so-called α -conjugate nuclei) are particularly stable, ${}^8\text{Be}$, ${}^{12}\text{C}$, ${}^{16}\text{O}$, ${}^{20}\text{Ne}$, . . . Figure 1.3, right-hand-side, shows the binding energy per nucleon plotted against the energy of the first excited state for a variety of nuclei. The nucleus ${}^4\text{He}$ stands out as being both

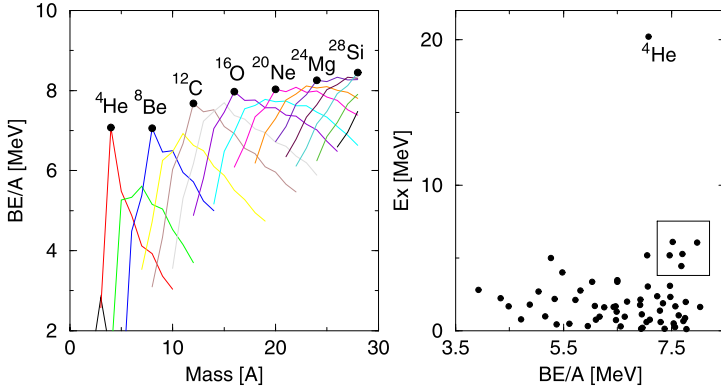
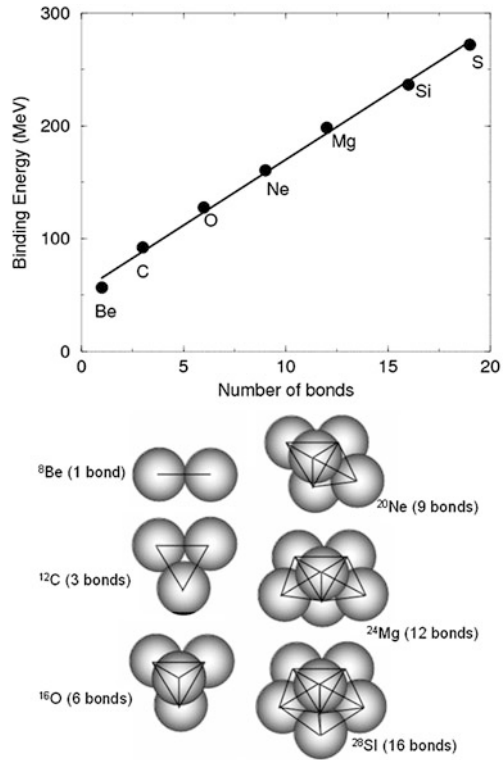


Fig. 1.3 (Left panel) Binding energy per nucleon of light nuclear systems (up to $A = 28$), the lines connect isotopes of each element. The “ α -particle nuclei” are marked by the circles. (Right panel) Excitation energy of first excited states plotted versus binding energy per nucleon for nuclei up to $A = 20$. Good clusters should have both high binding energies and first excited states. The nucleus ^4He is clearly an outstanding cluster candidate. The box drawn includes nuclei which may also form clusters: ^{12}C , ^{14}O , ^{14}C , ^{15}N and ^{16}O

stable and inert. These systems were also considered by Hafstad and Teller [3], who characterised the binding energy with number of “bonds” or interactions between the α -particles (Fig. 1.4). The rather linear relationship pointed to an apparently constant α - α interaction and the inertness of the α -particle in the ground states of these nuclei (it should be noted that this view is not one which is currently held, where the cluster structure is believed to be eroded in most ground-states). In essence, what this reveals is that the binding energies of such $N\alpha$ nuclei (N being an integer representing the number of α -particles) can be described in terms of $N(BE_\alpha) + N \cdot B_{\alpha\alpha}$, where BE_α is the binding energy of the α -particle and $B_{\alpha\alpha}$ is the energy associated with the α - α interaction. In turn this may be indicative of the importance of p - p , n - n and n - p correlation energies associated with occupation of common orbitals in nuclei with even and equal numbers of protons and neutrons (α -conjugate nuclei).

Earlier Morinaga had postulated, in a rather extreme prediction for the time, that it should be possible for the α -particles to arrange themselves in a linear fashion [4]. The idea that the cluster should not be manifest in the ground-state but emerge as the internal energy of the nucleus is increased was realised to be key in the 1960’s [5]. For a nucleus to develop a cluster structure it must be energetically allowed. Asymptotically, when the nucleus is separated into its cluster components an energy equivalent to the mass difference between the host and the clusters must be provided. There is an additional contribution which is the interaction between clusters which is required to fully separate them. In other words, the cluster structure would expect to be manifest close to, and probably slightly below, the cluster decay threshold. This was the view reached by Ikeda and co-workers, and is summarised in the diagram in Fig. 1.5. The diagram illustrates that each new cluster degree of freedom arises as the cluster decay threshold is approached, or crossed. Thus, there is the gradual transition from the compact ground-state to the full liberation of the $N\alpha$

Fig. 1.4 Binding energy per nucleon of $A = 4n$ nuclei versus the number of α - α bonds. The analysis by Hafstad and Teller [3] suggested that the ground states of $A = 4n$ (n being an integer, i.e. 1, 2, 3 ...), α -conjugate, nuclei could be described by a constant interaction energy scaled by the number of bonds. For ${}^8\text{Be}$ there is one bond, ${}^{12}\text{C}$ —3, ${}^{16}\text{O}$ —6, ${}^{20}\text{Ne}$ —9, ${}^{24}\text{Mg}$ —12 and for structural reasons (the geometric packing of the α -particles) ${}^{28}\text{Si}$ —16



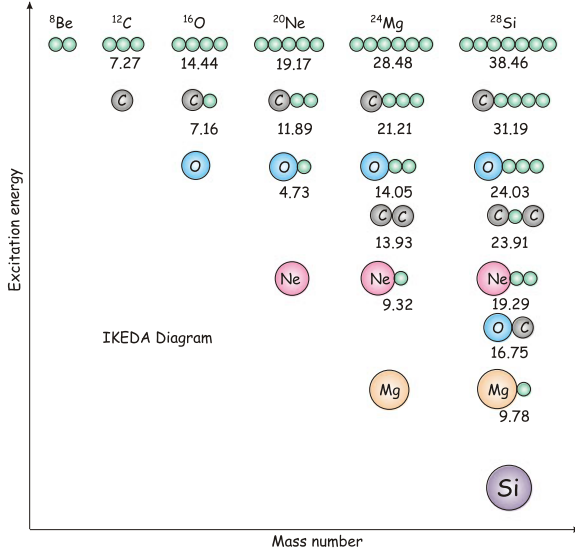
degree of freedom. Schematically, the diagram shows a linear arrangement of α -particles at the $N\alpha$ -limit, though this need not be the most stable configuration. In fact, it may be argued that the linear structure has an inherent instability [7], though many have interpreted this limit as representing a linear structure.

There is a second key ingredient whose role greatly influences the possible geometric arrangements of the clusters—and that is symmetries. These symmetries can be thought of as arising from the packing of the α -particles, but have a deeper origin which relates to the quantal properties of the system. In order to illustrate this, we start with an analysis of a rather simple and schematic approach to the nuclear mean-field, but one which is nevertheless rather powerful. In the application of the harmonic oscillator (HO) to the nuclear problem, it is assumed that each nucleon moves within a parabolic potential (i.e. a linear restoring force) created by the mean-interaction of all of the other constituents. The solution of the Schrödinger equation then yields the well known energy levels

$$E = \hbar\omega(n + 3/2) \tag{1.1}$$

for the three dimensional nucleus, where oscillations can be along any of the three cartesian coordinate axes and n is the number of oscillator quanta. If the nucleus, or equivalently potential, is deformed, for example stretched along the z -axis, then

Fig. 1.5 The Ikeda picture [5], from [6]. The diagram shows how the cluster degree of freedom evolves as the excitation energy increases. The *numbers* indicate the excitation energies at which the cluster structures should appear—these are the binding energies of the cluster components in the parent nucleus. The important concept relayed by this diagram is that a cluster degree of freedom is only liberated close to a cluster decay threshold. Thus, for heavy systems the $N\alpha$ degree of freedom only appears at the highest energies



the size of the potential in the x and y -directions must shrink in order to conserve the nuclear volume. The extended potential in the z -direction lowers the oscillation frequency and, for an axially symmetric potential, is increased in the perpendicular direction. Thus, the degeneracy implicit in (1.1), is removed and

$$E = \hbar\omega_{\perp}n_{\perp} + \hbar\omega_z n_z + \frac{3}{2}\hbar\omega_0 \quad (1.2)$$

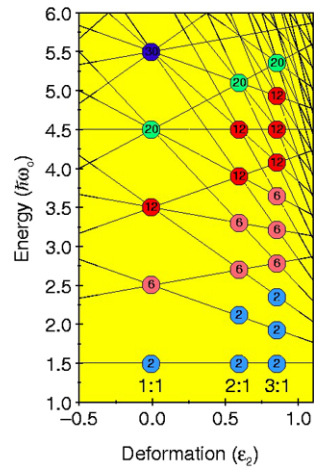
where the characteristic oscillator frequencies for oscillations perpendicular (\perp) and parallel (z) to the deformation axis are now required. These are constrained such that $\omega_0 = (2\omega_{\perp} + \omega_z)$, and the quadrupole deformation is given by

$$\varepsilon = \varepsilon_2 = (\omega_{\perp} - \omega_z)/\omega_0. \quad (1.3)$$

The total number of oscillator quanta is the sum of those on the parallel and perpendicular axes ($n_{\perp} + n_z$).

The characteristic energy levels of the deformed harmonic oscillator are shown in Fig. 1.6 [8]. The striking feature is the crossings of levels (regions of high degeneracy) which occur for axial deformations of $(\omega_{\perp} : \omega_z)$ 2:1 and 3:1. In fact, such degeneracies occur whenever the ratios $\omega_x : \omega_y : \omega_z = a : b : c$ where a , b and c are simple integers. Here shell structure is generated and corresponding *deformed* magic numbers emerge. In fact, the magic numbers reveal some particularly interesting behaviour. If rather than examining the magic numbers the sequence of degeneracies is explored, then the sequence of spherical degeneracies (2, 6, 12, 20, ...) is repeated twice at a deformation of 2:1 and three times at 3:1. This pattern would indicate two interacting spherical harmonic oscillator potentials at 2:1 and three at 3:1, etc. Here the symmetry appears within the magic numbers. These ideas were articulated mathematically by Nazarewicz and Dobaczewski [10].

Fig. 1.6 The deformed harmonic oscillator. The shell structure which appears at $\varepsilon_2 = 0$ vanishes as the potential is deformed, but reappears at deformations of 2:1, 3:1, etc. It is at these shell closures that cluster structure appears. The numbers in the circles indicate the degeneracy of the level scheme at the crossing points, from Ref. [9]



These symmetries have been explored elsewhere in detail in order to identify particular cluster partitions. Building on some of the earlier work of Bengtsson [11], Rae [12] focussed on the details of the deformed magic numbers in order to probe explicitly the cluster decompositions. These are shown in Table 1.1. Rae demonstrated that the deformed magic numbers could be expressed as the sums of spherical ones. This description locates at each deformation the associated cluster structure. At a deformation of 2:1 the superdeformed cluster states should be found in ${}^8\text{Be}$ ($\alpha + \alpha$), ${}^{20}\text{Ne}$ (${}^{16}\text{O} + \alpha$), ${}^{32}\text{S}$ (${}^{16}\text{O} + {}^{16}\text{O}$)... and at 3:1—hyperdeformation— ${}^{12}\text{C}$ ($\alpha + \alpha + \alpha$), ${}^{24}\text{Mg}$ ($\alpha + {}^{16}\text{O} + \alpha$), etc. Thus, the combination of the ideas of Rae and the Ikeda-picture permit the excitation-energy, deformation and single-particle configuration of cluster states to be determined.

The symmetries indicate a mapping between the shell structure and particular cluster states. However, the link runs deeper. We examine the rather trivial case of ${}^8\text{Be}$. The levels which are labelled with degeneracy 2 are those with the oscillator quantum numbers $[n_\perp, n_z] = [0, 0]$ and $[0, 1]$. Each of these levels would be occupied by pairs of protons and pairs of neutrons with their spins coupled to zero. The density distributions of the particles is given by the square of the corresponding wave-functions, $\varphi_{0,0}$ and $\varphi_{0,1}$. The overall ${}^8\text{Be}$ density is given by $|\varphi_{0,0}|^2 + |\varphi_{0,1}|^2$. These three components are shown in Fig. 1.7. The feature which emerges is one in which the density is double humped corresponding to the localisation of the protons and neutrons within two “ α -particles”. Interestingly, the observed distribution is generated by particles moving in an axially deformed potential, this generates a clustered density distribution which then in turn creates the mean-field in which the particles move. This latter field is not identical to the first. Clearly, to provide stable solutions, self consistent approaches are required. Some of these are described later (e.g. Antisymmetrized Molecular Dynamics (AMD) and Fermionic Molecular Dynamics (FMD)).

The above operation can be also applied to the 3:1 deformed shell closure, where we consider the three lowest orbits which are labelled with degeneracy 2. These

Table 1.1 Relationship between the deformed magic numbers at deformations of 2:1 and 3:1 and spherical cluster decompositions from [12]. For example, at a deformation of 2:1 the neutron and proton magic numbers 4, 10 and 16 can be decomposed into the spherical neutron and proton magic numbers $2 + 2$, $8 + 2$ and $8 + 8$. Thus, one would expect at a deformation of 2:1 the cluster structures $\alpha + \alpha$, $\alpha + {}^{16}\text{O}$ and ${}^{16}\text{O} + {}^{16}\text{O}$ to appear

$\omega_{\perp} : \omega_z = 2 : 1$			$\omega_{\perp} : \omega_z = 3 : 1$		
Magic numbers at 2:1	Spherical magic numbers	Associated cluster configuration	Magic numbers at 3:1	Spherical magic numbers	Associated cluster configuration
4	$2 + 2$	$\alpha + \alpha$	6	$2 + 2 + 2$	$\alpha + \alpha + \alpha$
10	$8 + 2$	${}^{16}\text{O} + \alpha$	12	$2 + 8 + 2$	$\alpha + {}^{16}\text{O} + \alpha$
16	$8 + 8$	${}^{16}\text{O} + {}^{16}\text{O}$	18	$8 + 2 + 8$	${}^{16}\text{O} + \alpha + {}^{16}\text{O}$
28	$20 + 8$	${}^{40}\text{Ca} + {}^{16}\text{O}$	24	$8 + 8 + 8$	${}^{16}\text{O} + {}^{16}\text{O} + {}^{16}\text{O}$
40	$20 + 20$	${}^{40}\text{Ca} + {}^{40}\text{Ca}$	36	$8 + 20 + 8$	${}^{16}\text{O} + {}^{40}\text{Ca} + {}^{16}\text{O}$

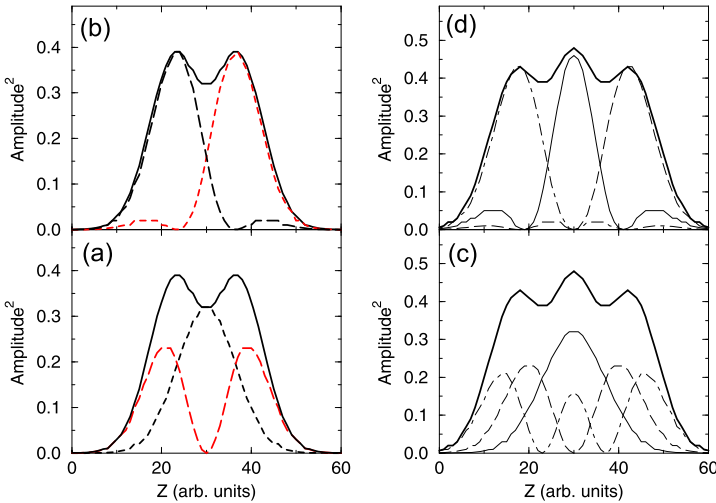
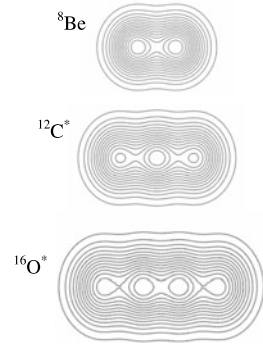


Fig. 1.7 The density corresponding to the HO configurations for (a) ${}^8\text{Be}$ and (c) ${}^{12}\text{C}$. In (a) the square of the $(n_x, n_y, n_z) = (0, 0, 0)$ and $(0, 0, 1)$ orbits are plotted as is their sum (*solid line*). The square of the $(0, 0, 0)$, $(0, 0, 1)$ and $(0, 0, 2)$ orbits together with their sum (*solid line*) are shown in (c). Parts (b) and (d) show the separation into the two and three-centered components, respectively. These show the individual α -particle densities

are the $[n_{\perp}, n_z] = [0, 0]$, $[0, 1]$ and $[0, 2]$ HO levels. Figures 1.7 and 1.8 shows the densities which correspond to these three orbits. What can be clearly observed is that at the deformation of 3:1 there is a three humped structure. In other words, it is possible to see the evidence for the systems division into three centers. As with the ${}^8\text{Be}$ case, it is possible to project out the “ α -particles” by appealing to the point symmetries of a three centered systems. If we employ the wave-functions containing

Fig. 1.8 The density of the three HO configurations associated with placing α -particles (pairs of protons and neutrons) in the orbits in Fig. 1.6 with degeneracy 2, at deformations of 2:1, 3:1 and 4:1. The densities correspond to the linear structures in the 2α , 3α and 4α systems ${}^8\text{Be}$, ${}^{12}\text{C}^*$ and ${}^{16}\text{O}^*$, respectively. In each case the presence of the α -particles is clear



these symmetries we can equate the number of nodes in the multi-centered wave-functions with those in the harmonic oscillator wave-functions under consideration;

$$\psi_{0,0} = \frac{1}{2}\phi_{\alpha(-)} + \frac{1}{\sqrt{2}}\phi_{\alpha(0)} + \frac{1}{2}\phi_{\alpha(+)} \quad (1.4)$$

$$\psi_{0,1} = \frac{1}{\sqrt{2}}\phi_{\alpha(-)} - \frac{1}{\sqrt{2}}\phi_{\alpha(+)} \quad (1.5)$$

$$\psi_{0,2} = -\frac{1}{2}\phi_{\alpha(-)} + \frac{1}{\sqrt{2}}\phi_{\alpha(0)} - \frac{1}{2}\phi_{\alpha(+)} \quad (1.6)$$

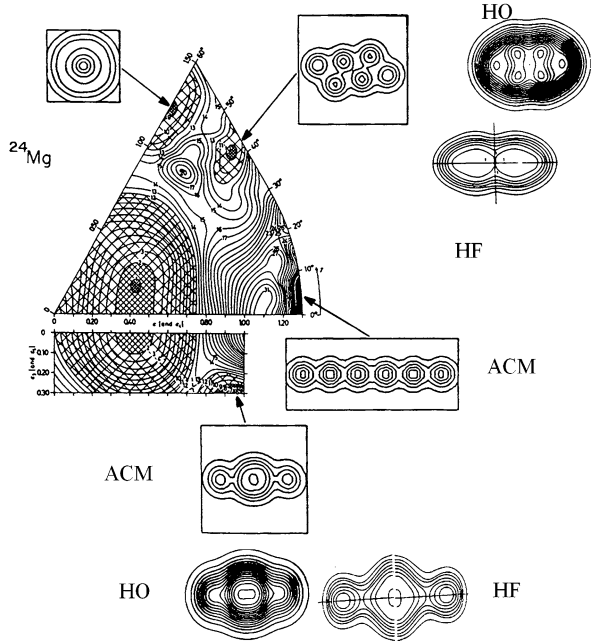
These can be solved for the three α -particle like wave-functions $\phi_{\alpha(-,0,+)}$. The resulting α -particle densities are shown in Figs. 1.7 and 1.8. The greater overlap of the “ α -particles” means that the central α -particle has additional higher order components (quantified in [9]).

Such an analysis may be performed universally across the deformed harmonic oscillator level scheme where ever shell structures arise and similar conclusions emerge; namely 2-fold clustering at a deformation at 2:1 and 3 at 3:1, etc. What is evident is that the cluster symmetries which are found in the HO are present *both* in degeneracies and densities. Figure 1.8 shows these symmetries for the first α -particle states appearing at deformations of 2:1, 3:1 and 4:1. Given the influence of the harmonic oscillator on more sophisticated nuclear models these cluster symmetries might be expected to be pervasive. The competition between the mean-field and clustering degrees of freedom is of great interest if the tendency of nuclei to fall either a shell-model or cluster-like description is to be probed. Itagaki and co-workers have recently explored this partition for a range of nuclei, e.g. Refs. [13–15].

Although more sophisticated models allow a more realistic description of the nucleus to be arrived at, the ideas developed here remain the leading order terms in our understanding of these nuclear states.

An example of this latter point may be found in a variety of calculations for ${}^{24}\text{Mg}$. Figure 1.9 shows a compilation of calculations for ${}^{24}\text{Mg}$. The central panel shows a Nilsson Strutinsky (NS) potential energy surface which is a macro-microscopic calculation which reveals a series of minima in the surface associated with meta-stable

Fig. 1.9 Comparison of a range of calculations of ^{24}Mg . The central panel shows a Nilsson Strutinsky calculation for the potential energy surface, the calculations around the outside show densities predicted by the Alpha Cluster Model (ACM), Hartree-Fock (HF) and Harmonic Oscillator (HO)



configurations. These may be linked directly with the appearance of shell structures in the deformed HO and also with Alpha Cluster Model (ACM) calculations in which the ^{24}Mg nucleus is described in terms of geometric arrangements of 6 α -particles—there is a one-to-one mapping between minima in the potential energy surface and the configurations found in the Alpha Cluster Model. In addition the densities for two structures found in Hartree-Fock (HF) calculations are shown—which bear a close resemblance to the structures found in the ACM. Finally, it is possible to extract from the NS calculations the underlying single-particle configuration and then this may be used to calculate the densities one would expect in the case of the harmonic oscillator (HO). Remarkably, these HO densities exhibit symmetries, or equivalently patterns, which are very strongly allied to those of the ACM. In other words, the symmetries that are associated with the arrangements of the α -particle clusters are pervasive in the mean-field type models. Thus, even if the α -particles themselves are not explicitly present within the nucleus their geometrical symmetries leave an imprint.

It should be noted that in the case of deformed states discussed here there exist two reference frames. The first is the intrinsic frame in which the coordinate system may be aligned with the deformation axis. In this case angular momentum of individual nucleons is not a good quantum number, only its projection onto the deformation axis. The second frame is the laboratory frame, which is the reference frame of the shell model—here angular momentum is a good quantum number. In calculations such as Hartree-Fock (HF) or Hartree-Fock-Bogoliubov (HFB), the latter including pairing, it is necessary to project out from the intrinsic states, states of good angular momentum (projection after variation). In the HF case this projection

is performed using the Peierls-Yoccoz procedure [16] and for the more complex case a technique introduced by Blatt [17]. The majority of the cluster structures presented in the present review correspond to intrinsic states. It is of course within this framework in which collective rotational energies have a natural description. In the case of light nuclei in which SU(3) symmetry is respected it is often possible to deduce the relationship between the intrinsic and laboratory descriptions, i.e. the shell model limit corresponding to various cluster structures [10].

1.4 More Sophisticated Models of Clustering

The deformed harmonic oscillator provides a very good basis for distilling the underlying behavior of light nuclei, but is schematic. If one is to make progress towards a more detailed understanding and the ability to reproduce experimental observables such as transition rates, radii and energies then models of greater sophistication are required. Historically many models have taken as a starting point an implicit assumption of the existence of clustering and developing an interaction between α -particles. In more recent times it has been realized that the α -particles within the nucleus cannot be considered to be truly inert, but that interactions will distort, polarize and modify the internal structure and that the real degrees of freedom are those of the nucleons. This section explores some of the developments of models and their merits.

1.4.1 Bloch-Brink Alpha Cluster Model (ACM)

The Alpha Cluster Model was first conceived of by Margenau [18] and then developed by Brink [19] drawing on the work of Bloch. Within the nuclear shell model the ${}^4\text{He}$ nucleus is constructed from $2p + 2n$ all within the $0s_{1/2}$ orbital. The principle construction of the alpha particle model is to build on this idea and that quartets are produced from pairs of protons and neutrons which are coupled to a total angular momentum of zero, i.e. they may be represented by a relative $0s$ -state. A collection of such quartet states may be modeled within the harmonic oscillator framework using

$$\phi_i(\mathbf{r}) = \sqrt{\frac{1}{b^3 \pi^{3/2}}} \exp\left[\frac{-(\mathbf{r} - \mathbf{R}_i)^2}{2b^2}\right]. \quad (1.7)$$

Here \mathbf{R}_i is the vector describing the location of the i th quartet, and $b = (\hbar/m\omega)^{1/2}$ is a scale parameter which determines the size of the α -particle. The overall wavefunction of the system formed from the collection of α -particles must then be antisymmetrized in recognition that the true degrees of freedom are fermionic. Corre-

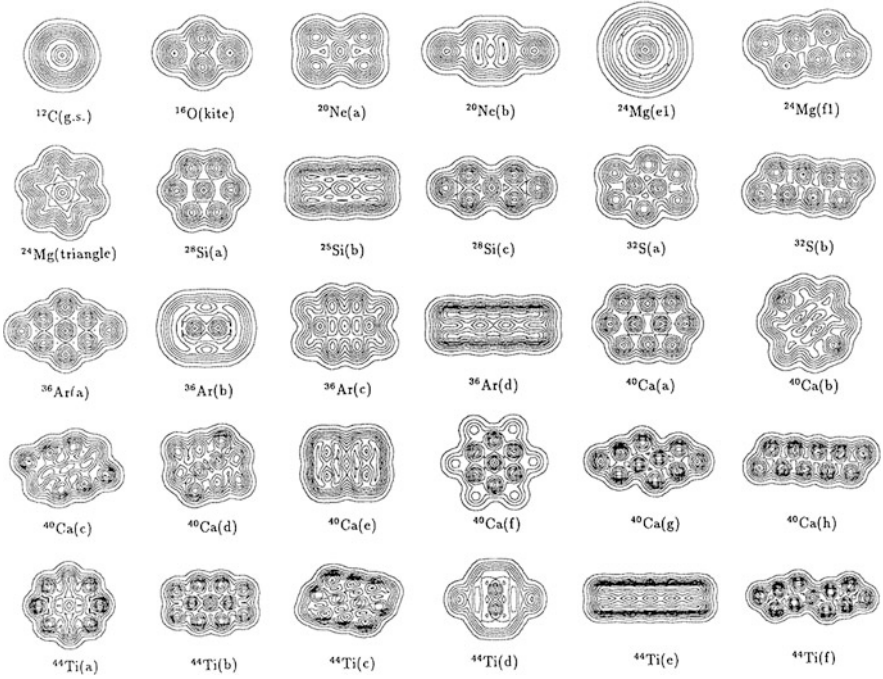


Fig. 1.10 Alpha Cluster Model (ACM) calculation for 2D structures in a range of light nuclei from Ref. [23]. See original work for further details

spondingly, the $N\alpha$ wave-function is then created using a Slater determinant

$$\Phi_{\alpha}(\mathbf{R}_1, \mathbf{R}_2, \dots, \mathbf{R}_N) = K \mathcal{A} \prod_{i=1}^N \phi_i(\mathbf{R}_i) \quad (1.8)$$

$\mathcal{A} \prod_{i=1}^N \phi_i(\mathbf{R}_i)$ being the Slater determinant wave-function (\mathcal{A} is the antisymmetrization operator accounting for the Pauli Exclusion Principle) and K a normalisation constant. The antisymmetrizer recognizes that the wave-function is actually composed of the fermionic degrees of freedom, albeit the fermions are embedded in the clusters. At short distances this will serve to break the α -particles. The Hamiltonian describing the total energy of the $N\alpha$ -system is

$$H = \sum_{i=1}^A T_i + \frac{1}{2} \sum_{i \neq j} [v(\mathbf{r}_i - \mathbf{r}_j) + v_c(\mathbf{r}_i - \mathbf{r}_j)] - T_{c.m.} \quad (1.9)$$

$T_{c.m.}$ is the center-of-mass energy and the α - α interactions are governed by the effective nucleon-nucleon potential $v(\mathbf{r}_i - \mathbf{r}_j)$ and Coulomb interaction $v_c(\mathbf{r}_i - \mathbf{r}_j)$.

The optimal arrangement of the α -particles is arrived at variationally, where the parameters which are optimised are the locations and size of the α -particles. This model has been applied extensively to light cluster systems by for example Brink [19], to the nucleus ^{16}O [20], a series of rather comprehensive set of calculations of the structure of ^{24}Mg by Marsh and Rae [21] (Fig. 1.9), linear arrangements of α -particles by Merchant [22] and finally a series of wide ranging calculations by Zhang et al. [23, 24], some of which are shown in Fig. 1.10. As was observed in Fig. 1.10, where the clusters were constrained to lie within a plane, many of the cluster structures are crystalline in nature.

As pointed out earlier there is a very strong mapping between the spatial symmetries found in these calculations and those which may be found in the densities associated with the deformed harmonic oscillator. In fact it is possible to deduce, in the limit that the separation of the α -particles tends to zero, the corresponding harmonic oscillator configurations. It is these oscillator configurations that then produce densities which emulate the patterns that are found in the Alpha Cluster Model.

1.4.2 Condensates and the THSR Wave-Function

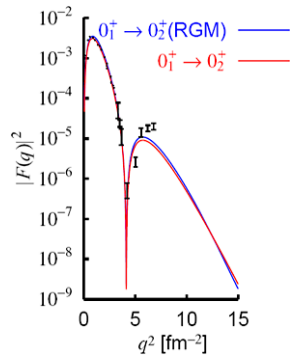
An intriguing possibility that the Alpha Cluster Model raises is that there may be a class of states in nuclei in which the separation of the α -particles is such that the internal structure of the α -particle is no longer so important. The conditions necessary to achieve this require that the nuclear radius is sufficiently large. Such a condition may be achieved close to the α -decay threshold, where in a state which is only weakly bound an α -particle may significantly tunnel into the barrier increasing the nuclear volume. Perhaps the best candidate for such behaviour is the 7.65 MeV, 0^+ , Hoyle-state in ^{12}C . From electron inelastic scattering measurements it is understood that the volume associated with the Hoyle state is some 3 to 4 times that of the ground-state. A further possibility then arises; if the state may be described by a collection of identical bosons is it possible for them to adopt bosonic symmetries and behave as an atomic Bose-Einstein condensate? In order to describe such a possibility, the Bloch-Brink wave-function (Sect. 1.4.1) has been adapted by Tohsaki, Horiuchi, Schuck and Röpke (THSR) to reflect the possible character of the state [25–27]. The condensed wave-function has the form

$$\begin{aligned} & \langle \mathbf{r}_1, \dots, \mathbf{r}_N | \Phi_{n\alpha} \rangle \\ &= \mathcal{A} \left[\phi_\alpha(\mathbf{r}_1, \mathbf{r}_2, \mathbf{r}_3, \mathbf{r}_4) \phi_\alpha(\mathbf{r}_5, \mathbf{r}_6, \mathbf{r}_7, \mathbf{r}_8) \phi_\alpha(\mathbf{r}_{N-3}, \dots, \mathbf{r}_N) \right] \end{aligned} \quad (1.10)$$

here the construction is for N nucleons grouped into quartets described by ϕ_α . The wave-function of the α -particle is given by

$$\phi_\alpha(\mathbf{r}_1, \mathbf{r}_2, \mathbf{r}_3, \mathbf{r}_4) = e^{-\mathbf{R}^2/B^2} \phi(\mathbf{r}_1 - \mathbf{r}_2, \mathbf{r}_1 - \mathbf{r}_3, \dots) \quad (1.11)$$

Fig. 1.11 The calculated inelastic form factor for electron inelastic scattering from the 0^+ ground state to the 0_2^+ excited state [29], compared with the experimental data from [30–32]



where $[\mathbf{R} = \mathbf{r}_1 + \mathbf{r}_2 + \mathbf{r}_3 + \mathbf{r}_4]/4$ is the c.o.m. coordinate of one α -particle and $\phi(\mathbf{r}_1 - \mathbf{r}_2, \mathbf{r}_1 - \mathbf{r}_3, \dots)$ is a Gaussian wave-function

$$\phi(\mathbf{r}_1 - \mathbf{r}_2, \mathbf{r}_1 - \mathbf{r}_3, \dots) = \exp(-[\mathbf{r}_1 - \mathbf{r}_2, \mathbf{r}_1 - \mathbf{r}_3, \dots]^2/b^2) \quad (1.12)$$

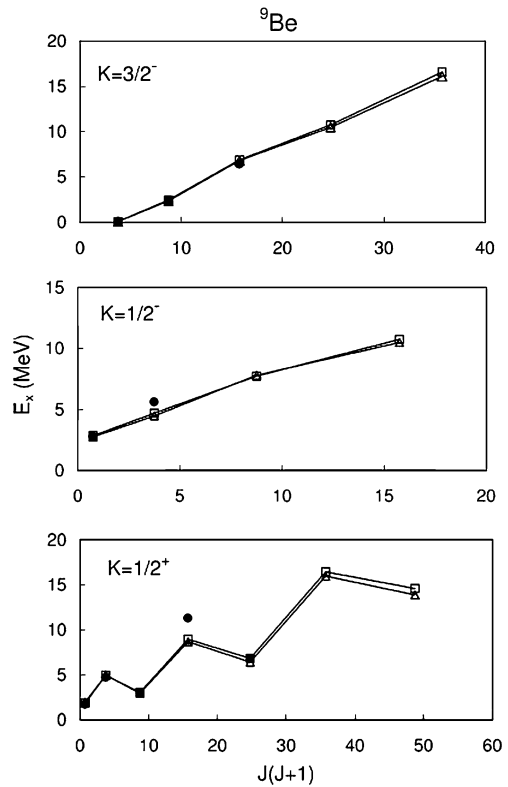
as in the ACM b is the size parameter of the *free* α -particle and $B (\gg b)$ is the parameter which describes the size of the common Gaussian distribution of the three α -particles. In the limit that $B \rightarrow \infty$ then the antisymmetrization operator \mathcal{A} ceases to be important and the wave-function (1.10) becomes the product of Gaussians, i.e. a wave-function describing a free α -particle gas [28]. The important feature is that in the limit that the volume becomes small the antisymmetrization takes over and the wave-function respects the internal fermionic degrees of freedom. In this way the wave-function is very similar to that of the Alpha Cluster Model, but possesses an additional variational degree of freedom.

One of the main successes of this model is that it manages to reproduce the form factor for the electron elastic excitation to the Hoyle-state without any arbitrary normalisation [29] (see Fig. 1.11). There is remarkable agreement with the experimental data, which would confirm the nature of the Hoyle-state as being both spatially extended and strongly influenced by an internal α -particle structure.

1.4.3 Microscopic Cluster Models

The Alpha Cluster Model produces a rather good picture of the nature of states within $A = 4n$ nuclei which condense out into collections of α -particles. However, although it antisymmetrizes the α -particles, their individual constituents are ignored, i.e. the internal excitations of the cluster. For clusters such as α -particles this may be a good approximation, but for other clusters this is not the case. Such shortcomings are addressed within the generator coordinate method (GCM) (also within the resonating group method (RGM)) [33–42]. Moreover, this approach permits reactions between the asymptotic clusters to be studied, as has been performed extensively by Baye and Descouvemont (e.g. Refs. [43–46]).

Fig. 1.12 The GCM calculations for ${}^9\text{Be}$ showing the three rotational bands associated with the $K^\pi = 3/2^-$ (π -configuration), $K^\pi = 1/2^+$ (σ -configuration) and $K^\pi = 1/2^-$ bands, from Ref. [47]. The experimental data are the *filled circles* and the *squares* and *circles* are the calculations for two different types of interaction



Within the RGM formalism the wave-function describing the A nucleons, separated into two clusters with A_1 and A_2 constituents, may be written as,

$$\Psi(\mathbf{r}_1, \mathbf{r}_2, \dots, \mathbf{r}_A) = F(\mathbf{R}_{cm}) \hat{A} \{ \phi_1(\xi_1) \phi_2(\xi_2) g(\mathbf{R}) \} \quad (1.13)$$

here $F(\mathbf{R}_{cm})$ describes the motion of the center of mass of the nucleus, ϕ_i represent antisymmetrized internal states of the two clusters (whose internal coordinates are described by ξ_i), $g(\mathbf{R})$ is a function of the relative motion of the two clusters (so that the relative coordinate \mathbf{R} is given by $(1/A_1) \sum_{i=1}^{A_1} \mathbf{r}_i - (1/A_2) \sum_{j=1}^{A_2} \mathbf{r}_j$) and \hat{A} is the antisymmetrization operator which exchanges nucleons between the two clusters. The great advantage of this approach is the fact that the constituents of the clusters are fully antisymmetrized and that the center-of-mass of the system is correctly treated so that the quantum numbers produced have a realistic meaning in terms of the asymptotic fragments. The above corresponds to the single-channel form of the RGM, if excitations of the cluster cores are required then so is a multi-channel approach.

An impressive demonstration of the GCM can be found in the calculations of the structure of the microscopic structure of ${}^9, {}^{10}, {}^{11}\text{Be}$ isotopes using $2\alpha + Xn$ configurations by Descouvemont [47]. The calculations for ${}^9\text{Be}$ reproduce almost per-

fectly the rotational bands in this system. In particular, the Coriolis decoupling of the $K^\pi = 1/2^+$ band is found (see Fig. 1.12). These GCM calculations reproduce the characteristics of the molecular states in the nuclei $^9,^{10},^{11}\text{Be}$. In this instance the neutrons reside in molecular orbits whereby they are exchanged between the two α -particle cores— π -orbit for the ground state band and σ for the excited states (see Sect. 1.7).

In recognition of this molecular behaviour, some approaches employ such orbitals explicitly in defining the basis states for the calculation of the structural properties. For example, this molecular-orbit (MO) approach has been used to calculate the properties of the neutron-rich beryllium [48–50] and carbon isotopes [51]. Here the molecular orbits are formed from linear combinations of p -orbitals based around α -particle centers. The MO framework also allows collisions between two nuclei to be considered, for example in the generalized two-center cluster model (GTCM), using a basis function of the form

$$\Phi_{m,n}^{J^\pi K} = \hat{P}_K^{J^\pi} \cdot \mathcal{A} \{ \psi_L(\alpha) \psi_R(\alpha) \phi(m) \phi(n) \}, \quad (1.14)$$

the formation of resonances in ^{10}Be from $^6\text{He} + ^4\text{He}$ has recently been considered [52]. Here $\psi_{L,R}(\alpha)$ is the wave-function of the left/right (L/R) α -particle and $\phi(m, n)$ are the molecular wave-functions of the neutrons. $\hat{P}_K^{J^\pi}$ and \mathcal{A} are the parity projection and antisymmetrisation operators ensuring states have good angular momentum (J), angular momentum projection (K) and parity (π). Rather interestingly, these calculations indicate that in the inelastic scattering reaction $^4\text{He} + ^6\text{He} \Rightarrow ^4\text{He} + ^6\text{He}(2^+)$ an avoided crossing which takes place between different molecular configurations that a Landau-Zener type transition [53, 54] is responsible for the inelastic scattering in the $L = 1$ channel. In other words the formation of molecular configurations in the scattering process can have a marked impact on the elastic and inelastic scattering processes.

1.4.4 Antisymmetrised Molecular Dynamics (AMD) and Fermionic Molecular Dynamics (FMD)

The AMD approach, which has been comprehensively reviewed recently by Kanada-En'yo and Horriuchi [55], has many important advantages over microscopic cluster models, but the most significant is that there are no assumptions made about the cluster or the relative coordinates between clusters. The model is one in which the nucleonic degrees of freedom are explicitly included and the A -nucleon wave-function is then antisymmetrised again via a Slater determinant:

$$\Phi_{AMD}(\mathbf{Z}) = \frac{1}{\sqrt{\mathbf{A}!}} \mathcal{A} \{ \varphi_1, \varphi_2, \dots, \varphi_{\mathbf{A}} \}. \quad (1.15)$$

In this way the model resembles the Bloch-Brink cluster model, but contains as degrees of freedom the nucleons and releases the constraint that α -particles be preformed. Consequently, clusters emerge without being imposed. The φ_i are Gaussian

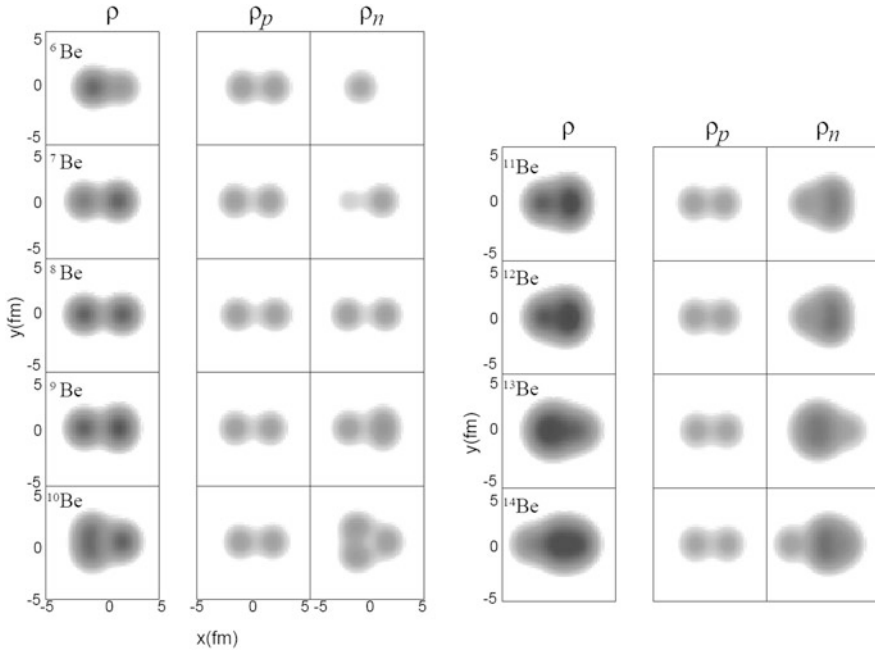


Fig. 1.13 The density distributions of the ground-states of the beryllium isotopes calculated within the framework of the AMD. The *first column* shows the total nucleon density (ρ) and the *middle and right-hand columns* the proton (ρ_p) and neutron densities (ρ_n). From [55]

wave-packets in space, $\phi_{\mathbf{x}_i}(\mathbf{r}_j) \propto \exp(-\nu(\mathbf{r}_j - \mathbf{X}_i/\sqrt{\nu})^2)$, but also possess spin (χ_i) and isospin character (τ_i): $\varphi_i = \phi_{\mathbf{x}_i} \chi_i \tau_i$. The wave-function is parameterized in terms of a complex set of variables \mathbf{Z} describing the spin and geometry of the wave-function. The energy of the system is computed, variationally, utilizing an *effective* nucleon-nucleon interaction (see Ref. [55] for more details). The flexibility of this approach allows a suitable description of cluster and shell-model type systems, alike, and the structure emerges naturally from the details of the nucleon-nucleon interaction under the guidance of the Pauli Exclusion Principle.

An example of the appearance of the precipitation of clusters from the nucleon-nucleon interaction within the framework of the AMD is shown in Fig. 1.13 for the beryllium isotopes ${}^6\text{--}14\text{Be}$. All isotopes possess a proton distribution which is prolate and clustered. The role of the neutrons is clear. When the neutron number is the same as that of the protons (${}^8\text{Be}$) the separation of the proton-cores is maximal (maximum clustering), whereas neutrons in more spherical distributions cause the separation of the proton centers to be reduced. This model has been widely applied, but with a particular focus on the Li, Be, B and C isotopes, see Ref. [55] and references therein. In general the model reproduces well both experimental binding energies, transition rates, radii and moments. Figure 1.14 shows some examples of the rather close agreement between the AMD calculations and the experimental electric quadrupole moments and electromagnetic transition rates.

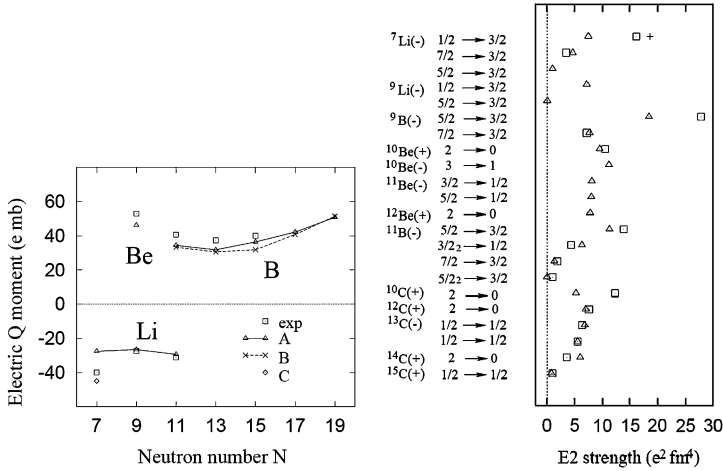


Fig. 1.14 (Left) Electric quadrupole moments for Li, Be and B isotopes. The *squares* are experimental data and other symbols are the AMD calculations with slightly different interactions or constructions. (Right) $E2$ transition strengths for Li, Be, B and C isotopes. The *squares* are the experimental data points, the other symbols are the AMD calculations. See Ref. [55] for further details

An alternate approach to AMD which contains an additional degree of freedom, namely each nucleon is represented by two Gaussian wave-packets, is fermionic molecular dynamics (FMD) [56]. Moreover, the interaction employed (Unitary Correlation Operator Method—UCOM) includes a tensor component. The features of these calculations essentially coincide with those of the AMD, but the variable Gaussian width should allow, in principle, a better description of shell-model like states and should potentially provide a better description of weakly bound states. The recent calculations for the structure of the 7.65 MeV state in ${}^{12}\text{C}$ are of particular note [57].

1.4.5 *Ab Initio Type Models*

Ultimately, it is important to be able to push beyond models which either employ assumptions of preformed clusters or effective interactions. The Green's Function Monte Carlo (GFMC) method, described earlier, uses realistic two-body interactions with a parameterization of the 3-body force. Not only does this method reproduce the properties of light nuclei up to $A = 12$ rather precisely, but, as shown in Fig. 1.2, also indicates the emergence of cluster like structures in nuclei such as ${}^8\text{Be}$ [1].

Another approach which attempts to extend beyond the shell model is the no-core shell model (NCSM) in which realistic interactions are used but with a set of basis states which are harmonic oscillator states [58]. This approach provides an

analytic basis for the construction of the many-body Slater determinants. The downside is that HO wave-functions do not have the appropriate asymptotic behavior (as a function of r), which means that they tend not to be a good description of weakly bound systems, and also all states of the system end up being effectively bound due to the nature of the potential. As its name suggests the interaction between all nucleons is taken into account (rather than the valence nucleons beyond the closed shell) and it may use a variety of interactions including those used in the GFMC approach (the Argonne potentials) and those from Effective Field Theory (EFT).

In this latter case the interaction is grown from QCD by including various types of exchange processes which in leading order include one pion exchange terms. Higher order corrections include more complex processes for example next to leading order (NLO) includes 2 pion exchange and terms which correspond to pions being radiated and absorbed by a single nucleon which interacts with a second via pion exchange (called renormalisation of 1 pion exchange). Current models extend to N3LO (next to, next to, next to leading order) which amongst other components would include 3 pion exchange components [59, 60] and even N4LO.

Calculations of the states of ^{12}C using the no-core shell model [61, 62] struggle to reproduce the excitation of the 7.65 MeV, 0^+ , Hoyle state without an extension of the basis to include excitations to HO levels at very high energies (large $\hbar\omega$). The Hoyle-state has long been known to possess a cluster-like structure and the failure of the NCSM to capture the detail of this state without a significant expansion of the basis is thus not surprising. In fact, this may be taken as a signature of clusterization.

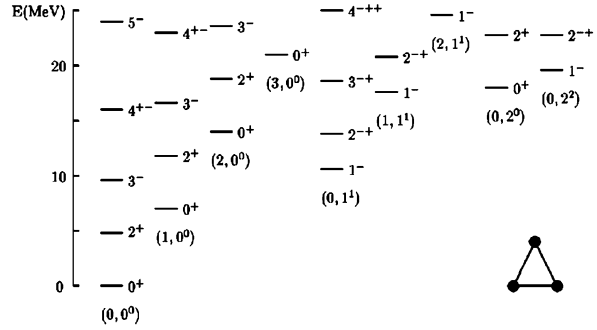
Finally, a rather promising development is the use of chiral EFT interactions in lattice based calculations. A series of calculations of the structure of the states in ^{12}C , including the Hoyle-state, have been performed. These point to both clusterization and a rather different structure of the ^{12}C ground and excited states [63–65]. The lattice spacing used in these calculations remains rather coarse, but further optimization has the potential for providing great insight into the structure of light clustered systems and their reactions.

1.5 Experimental Examples of Clustering

1.5.1 The Example ^8Be

The ground-state of ^8Be is unbound to 2α decay by 92 keV, and has a lifetime of $\sim 10^{-16}$ s. It has a first excited 2^+ state at 3.03 MeV with a width of 1.51 MeV and a 4^+ state at 11.35 MeV with a width of 3.5 MeV. These three states have an energy separation which is consistent with a rotational behaviour given by $\hbar^2 J(J+1)/2\mathcal{I}$, where \mathcal{I} is the moment of inertia. The value for the moment of inertia that one extracts is consistent with the picture of two touching α -particles, an essentially super-deformed nucleus. Indeed the Green's Function Monte Carlo calculations [1] reproduce the spectrum of excited states which reinforces this interpretation. There appears to be little doubt that clusterisation is a dominant factor in the structure of the ^8Be nucleus.

Fig. 1.15 Spectrum of the energy levels of an equilateral triangle configuration. The bands are labeled by $(v_1; v_2^l)$ [66]



1.5.2 The Structure of ^{12}C

If the structure of the ^{12}C ground state is influenced by clustering or the symmetries thereof, then the system can be constructed from a variety of geometric arrangements of three α -particles. It might be expected that the compact equilateral-triangle arrangement is the lowest energy configuration. Such an arrangement possesses a D_{3h} point group symmetry. The corresponding rotational and vibrational spectrum is described by a form [66]

$$E = E_0 + Av_1 + Bv_2 + CL(L + 1) + D(K \pm 2l)^2 \quad (1.16)$$

where $v_{1,2}$ are vibrational quantum numbers, and v_2 is doubly degenerate; $l = v_2, v_2 - 2, \dots, 1$ or 0, L is angular momentum, M its projection on a laboratory fixed axis and K a body-fixed axis [66]. A, B, C and D are adjustable parameters. The spectrum of states predicted by the choice $A = 7.0, B = 9.0, C = 0.8$ and $D = 0.0$ MeV is shown in Fig. 1.15.

The ground state band, $(v_1; v_2^l) = (0, 0^0)$, contains no vibrational modes and coincides well with the observed experimental spectrum. Here the states correspond to different values of K ($K = 3n, n = 0, 1, 2, \dots$) and L . For $K = 0, L = 0, 2, 4$ etc., which is a rotation of the plane of the triangle about a line of symmetry, whereas for $K > 0, L = K, K + 1, K + 2, \dots$. In the present case, $K = 0$ or 3 is plotted with the parity being given by $(-1)^K$. The $K = 0$ states coincide well with the well-known 0^+ (ground-state), 2^+ (4.4 MeV) and 4^+ (14.1 MeV) states. The $K = 3$ states correspond to a rotation about an axis which passes through the center of the triangle, with each of the α -particles carrying one unit of angular momentum. The first state has spin and parity 3^- and coincides with the 9.6 MeV, 3^- , excited state. The next such state would be $K = 6, J^\pi = 6^+$. A prediction of this model is that there should be a 4^- state almost degenerate with the 4^+ state. A recent measurement involving studies of the α -decay correlations indicated that the 13.35 MeV unnatural-parity state possessed $J^\pi = 4^-$ [67]. The close degeneracy with the 14.1 MeV 4^+ state would appear to confirm the D_{3h} symmetry. The rotational properties of these states are given by

$$E_{J,K} = \frac{\hbar^2 J(J + 1)}{2\mathcal{I}_{\text{Be}}} - \frac{\hbar^2 K^2}{4\mathcal{I}_{\text{Be}}} \quad (1.17)$$

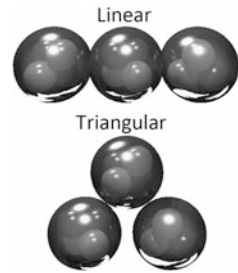
where \mathcal{I}_{Be} is the moment of inertia corresponding to two touching α -particles which can be determined from the ${}^8\text{Be}$ ground-state rotational band [3].

Historically, one of the pre-eminent tests of our understanding of the structure of light nuclei lies in the nature of the second excited state in ${}^{12}\text{C}$. This system resides at the limits of many of the *ab-initio* approaches. This state has character $J^\pi = 0^+$ and lies at $E_x = 7.65$ MeV. It is known as the Hoyle-state as it was predicted by Fred Hoyle [68, 69] as a solution to the discrepancy between the observed and predicted abundance of ${}^{12}\text{C}$. ${}^{12}\text{C}$ is synthesized in the triple- α process, whereby the two α -particles briefly fuse to make ${}^8\text{Be}$ and at sufficient densities there is a finite probability of capturing a third α -particle to form ${}^{12}\text{C}$. The 7.65 MeV state serves as a *doorway* resonance, substantially enhancing the reaction-rate. Without this resonance, or even if its energy were slightly different, the abundance of carbon would be dramatically reduced as would that of carbon based life-forms.

In the description illustrated in Fig. 1.15 the 0^+ state at 7.65 MeV corresponds to a vibrational mode ($v_1 = 1$). The coupling of rotational modes would then produce a corresponding 2^+ state at 4.4 MeV above 7.65 MeV, i.e. 12.05 MeV. There is no known 2^+ state at this energy, pointing to the more complex structure of this state. If the 7.65 MeV state in ${}^{12}\text{C}$ has a structure similar to that of the ground-state then a 2^+ state close to 12 MeV is expected. The closest state which has been reported with these characteristics is at 11.16 MeV [70]. This state was observed in the ${}^{11}\text{B}({}^3\text{He}, d){}^{12}\text{C}$ reaction, but has not been observed in measurements subsequently. A re-measurement of this reaction using the K600 spectrometer at iThemba in South Africa demonstrates that the earlier observation of a state at 11.16 MeV was an experimental artifact and no such state exists [71]. This introduces an interesting set of possibilities which lie at the heart of uncovering the structure of the Hoyle-state. If the Hoyle-state is more deformed than the ground-state, and the system behaves in a rotational fashion, then the 2^+ state would be lower in energy and an alternative possibility is that the Hoyle-state possesses no collective excitations. It has been suggested that due to the close proximity of the Hoyle-state close to the 3α -decay threshold, bound only by the presence of the Coulomb barrier, that the system obtains a bosonic rather than fermionic identity and that the α -particle bosons behave like a weakly interacting bosonic gas or even a bosonic condensate [25]. The resolution of the structure may follow from the identification of the 2^+ excitation—or otherwise.

Recent studies of the ${}^{12}\text{C}(\alpha, \alpha')$ [72–74] and ${}^{12}\text{C}(p, p')$ [75, 76] reactions indicate the presence of a 2^+ state close to 9.6–9.7 MeV with a width of 0.5 to 1 MeV. The state is only weakly populated in these reactions, presumably due to its underlying cluster structure, and is broad. Consequently, its distinction from other broad-states and dominant collective excitations (e.g. the 9.6 MeV, 3^-) makes its unambiguous identification challenging. Further, and perhaps definitive, evidence for such an excitation comes from measurements of the ${}^{12}\text{C}(\gamma, 3\alpha)$ reaction performed at the HIGS facility, TUNL [77] in the US. Here a measurable cross section for this process was observed in the same region of 9–10 MeV which cannot be attributed to known states in this region. Furthermore, the angular distributions of the α -particles are consistent with an $L = 2$ pattern, indicating a dominant 2^+ component. Based

Fig. 1.16 Different arrangements of α -particles. The closest possibility fitting the experimental data is the triangular arrangement



on a rather simple description of this state in terms of three α -particles with radii given by the experimental charge radius (see Fig. 1.16 for possible arrangements), it is possible to use the 2 MeV separation between the Hoyle-state and the proposed 2^+ excitation to draw some conclusions as to the arrangements of the clusters. This would indicate that rather than a linear arrangement of the three clusters, a more appropriate description would be a loose arrangement of the α -particles in something approaching a triangular structure.

A natural extension of such a conclusion is that there should also be a collective 4^+ state. Using the simple $J(J + 1)$ scaling, a 4^+ excitation close to $E_x(^{12}\text{C}) = 14$ MeV would be expected. Recent measurements of the two reactions $^9\text{Be}(\alpha, 3\alpha)n$ and $^{12}\text{C}(\alpha, 3\alpha)^4\text{He}$ have been performed [78]. These measurements indicate a candidate state close to 13.3 MeV with a width estimated to be 1.7 MeV. It is believed that this is not a contaminant and is observed with similar properties in all spectra. Angular correlation measurements made using the ^{12}C target are not definitive, but indicate a 4^+ assignment.

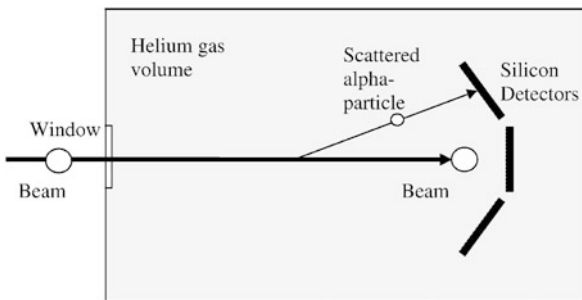
1.6 Experimental Techniques—Break-up and Resonant Scattering Reactions

A determination of the structure of light nuclei above the particle decay threshold, where gamma-decay ceases to be dominant, is challenging. In order to characterize the nature of excited states, the energies, total and partial widths and spins and parities should be determined. There are few experimental techniques which permit all of these quantities to be determined simultaneously.

1.6.1 Resonant Scattering

One approach which recently has found greater favor is thick target resonant scattering [79]. Here a beam passes through a thick target losing energy as it traverses the medium. By far the majority of the interactions are with the atomic electrons slowing the beam, however occasionally a nuclear interaction takes place. The cross section for resonant capture reaches hundreds of millibarns. The resonance in the

Fig. 1.17 Resonant scattering using a thick helium target



target-beam composite system then can decay either back into the entrance channel or into other final states. The fact that the beam energy is continuously varying in the medium means that the center-of-mass energy is scanned—this results in a technique which is considerably more efficient than the traditional excitation function measurements, where the beam energy must be re-tuned for each data point. For elastic resonant scattering involving a projectile and an α -particle target the cross section is given by

$$\sigma(E) = \pi \lambda^2 \frac{2J + 1}{2J_1 + 1} \frac{\Gamma_\alpha^2}{(E - E_r)^2 + (\Gamma/2)^2} \tag{1.18}$$

where J is the spin of the resonance, J_1 is the spin of the projectile, E_r the energy of the resonance and Γ and Γ_α the total and α -partial widths, respectively. The cross section thus scales linearly with J and quadratically with Γ_α —the greater the degree of clusterization the larger the partial width and the larger the cross section. Resonant elastic scattering from an α -particle target is thus ideally matched to the study of cluster states. For inverse kinematics, where the beam is heavier than the target, the resolution with which it is possible to reconstruct excited states can exceed the energy resolution of the detection system.

The experimental approach is illustrated in Fig. 1.17. The beam, of energy typically a few MeV/u, passes through a window, which is typically Havar or Mylar of thickness 5 μm , to contain the helium gas with pressures up to about 1 atmosphere. The beam loses energy and undergoes energy-loss straggling as it passes through the window and the target gas. This leads to a loss in resolution. As the beam traverses the gas volume it again decelerates until finally it is stopped. The range of the beam is adjusted via the variation of the gas pressure, such that the beam stops immediately in front of the detectors. Of course if the range exceeds the distance to the detectors and the beam is sufficiently intense the detectors will be destroyed. Any interaction with an α -particle along the path of the beam has the potential to result in elastic scattering—either resonant or non-resonant. These two processes will interfere with each other. For center-of-mass angles close to 180 degrees the α -particles will be emitted in the same direction as the beam and since typically the beam has a mass and charge in excess of α -particles, the scattered α -particles have a lower energy loss in the gas and thus can reach the detectors. The main drawback for this approach arises when a helium gas target is extended and in this instance the

precise location of the interaction cannot be determined. This means that there is an ambiguity in the emission angle when the α -particle is detected in the silicon array. Only at zero degrees (the beam direction) does this problem vanish. Here it is possible to establish the location of the interaction within the gas volume and thus correct for the energy loss of the α -particle as it traversed the gas and hence the energy upon emission. This then permits the excitation energy of the composite target+projectile system to be established. For emission away from zero degrees the path length of the beam and emitted α -particle through the gas is harder to establish—though it is possible to develop iterative techniques to address this. The excitation energy resolution away from zero degrees tends to be correspondingly degraded.

The study of resonances in the $^{18}\text{O} + \alpha$ system by Rogachev et al. [80] is shown in Fig. 1.18. This shows the energy spin systematics of the resonances observed in ^{22}Ne obtained using this technique [80]. The systematics of the energies in the bands are compared with those for ^{20}Ne and show a similar rotational trend, but for each rotational level the states are split into two components. It is possible that the states observed have a molecular structure in which two neutrons are exchanged between α -particle and ^{16}O cores.

1.6.2 Break-up Measurements

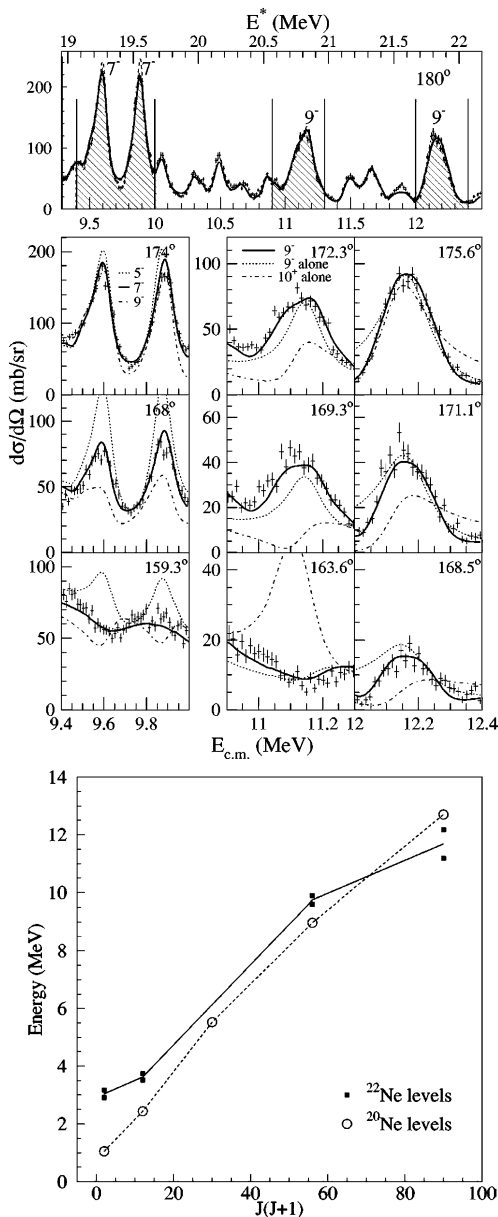
The utility of break-up reactions in the study of nuclear clustering has been reviewed in Ref. [81]. In this approach, states above particle decay channels with a particular type of cluster structure are observed to decay into the cluster components. The argument being, that if the states have large cluster widths then they are more likely to decay in a manner respecting this structure and hence the break-up spectrum is most strongly populated by cluster states. The reaction populating such states may range from inelastic scattering to transfer. Figure 1.19 shows the sequence of states populated in the $^{12}\text{C}(^{24}\text{Mg}, ^{12}\text{C} + ^{12}\text{C})^{12}\text{C}$ inelastic scattering reaction. The experimental technique employed is akin to invariant mass spectroscopy and has been termed resonant particle spectroscopy. It involves the simultaneous detection of the two decay products (in this case two ^{12}C nuclei) using detectors which are capable of measuring both the energy and emission angles of the particles. If the detection system is capable of also determining the mass of the fragments then the momentum of the two fragments may be established. Using the principles of conservation of momentum it is possible to calculate the momentum of the ^{24}Mg nucleus before decay and hence its kinetic energy, $E(^{24}\text{Mg})$. The excitation energy then follows

$$E_x = E(^{12}\text{C}_1) + E(^{12}\text{C}_1) - E(^{24}\text{Mg}) - Q_{bu} \quad (1.19)$$

where Q_{bu} is the breakup threshold, which in this instance is -13.93 MeV. Momentum conservation also permits the energy of the recoil to be calculated and hence the three-body reaction Q -value to be calculated. In this way it is also possible to select events in which the decay proceeds only to the ground states of the three final-state

Fig. 1.18 Excited states of ^{22}Ne , populated in $^{18}\text{O} + \alpha$ scattering. The energy above threshold is given as $E_{c.m.}$.

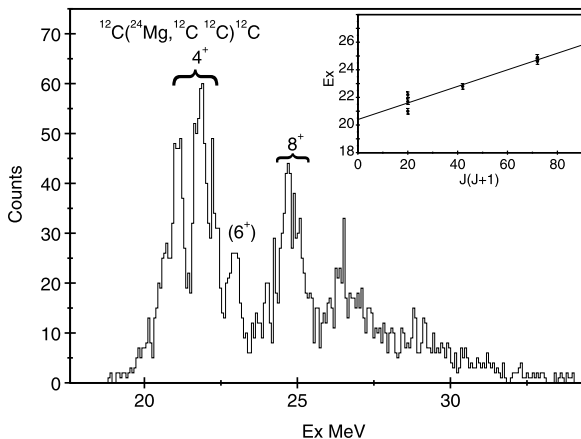
Upper figure top panel: excitation functions of resonant elastic scattering at different cm -angles as indicated. *Upper figure lower panel:* Details of the upper part with enhanced regions, showing the fits used to determine the spin values as indicated. *Lower figure:* plots of the observed excitation energies as function of spin ($J(J + 1)$) for ^{22}Ne compared to corresponding values of ^{20}Ne , from Ref. [80]



^{12}C nuclei. This is important otherwise the excitation energy spectrum contains an ambiguity corresponding to decays proceeding to the ^{12}C first excited state (2^+ , 4.4 MeV).

A second advantage of being able to determine the fact that all three final state ^{12}C nuclei were produced in their 0^+ ground-states is that the technique of angular

Fig. 1.19 States in ^{24}Mg decaying into two ^{12}C nuclei populated in the $^{12}\text{C}(^{24}\text{Mg}, ^{12}\text{C} + ^{12}\text{C})^{12}\text{C}$ inelastic scattering reaction. The *horizontal axis* is the excitation energy of the ^{24}Mg nucleus and the *vertical axis* represents the counts per bin. The *inset* shows the energy-spin systematics of the states which appear to follow a rotational behaviour consistent with a $^{12}\text{C} + ^{12}\text{C}$ cluster structure



correlations may then be utilized. If all initial and final state nuclei are spin zero, then the mathematical form describing the angular distribution of the decay products is essentially that described by Legendre polynomials [82]. Given that there are two center-of-mass frames, the first associated with the inelastic scattering of the $^{24}\text{Mg}^*$ nucleus and the second describing the decay of the $^{24}\text{Mg}^*$ nucleus into two ^{12}C nuclei, there are two sets of angles and it is the correlation between these two processes which reveals the spin of the decaying $^{24}\text{Mg}^*$ excited state. The angular correlation technique in principle permits quasi model independent spin determinations.

The breakup technique thus allows excitation energies and spins to be determined. However, it is often difficult to achieve excitation energy resolutions less than 100 keV and hence measuring the natural widths of states is challenging and in order to know the partial widths the excitation probability must also be determined which is also challenging. In some instances this has been overcome for example using a spectrometer to measure the recoil particle, e.g. [83], in order to determine the nature of the excitation energy spectrum prior to decay.

1.7 Beyond α -Clusters—Valence Neutrons and Molecules

Alpha-conjugate nuclei are clearly a very small subset of all those which exist in nature and in this instance that the clusterisation arises from the rather special properties that stem from the common orbitals in the mean-field limit. As has been observed this gives rise to particular symmetries which pervade both the mean-field and cluster model limits and may be interpreted as spatially localized clusters. When one moves away from such even $N, Z, N = Z$ nuclei then some of the energetic advantage associated with the α -particle are lost and the symmetries disturbed. The important question is, does clustering vanish at this point or does it remain influential even at the drip-lines? As described earlier on, there is evidence of the importance of correlations, or clustering, even at the drip-lines. The properties of ^6He may

be traced both to the reliance of the α -particle and the effect of correlations between the neutrons [84]—the removal of one of the neutrons leaves the unbound ${}^5\text{He}$. The presence of the α -particle also affects the binding of the two neutrons; the di-neutron is unbound. Understanding the behaviour of such finely balanced nuclei right at the drip-lines can give a deep insight into the intricacies of the strong nuclear force. In this instance it is the α -particle which forms part of the building block. Similarly the nuclei ${}^6,{}^7\text{Li}$ possess $\alpha + d$ and $\alpha + t$ structures, respectively. The ${}^6\text{Li}$ ground-state spin of 1^+ would correspond to the $J^\pi = 0^+$ α -particle with a deuteron ($J^\pi = 1^+$) with a relative motion described by $L = 0$ (ignoring the small D -state component).

The first significant attempt to deal with the additional degrees of freedom that valence nucleons bring to systems was that of Hafstad and Teller [3]. This seminal piece of work set the ground rules for this field. These authors considered the sequence of nuclei, ${}^5\text{He}$, ${}^9\text{Be}$, ${}^{13}\text{C}$ and ${}^{17}\text{O}$. The binding energies of these $4n + 1$ nuclei ($n = 1, 2, 3, \dots$) depend on the α - α interaction energy, but also the character of the valence neutrons. The binding energy of the ${}^5\text{He}$ nucleus reflects the α - n interaction, whereas the $\alpha + n + \alpha$ nucleus ${}^9\text{Be}$ whilst containing similar terms in the Hamiltonian was recognised as having a contribution from an *exchange* interaction. Here, the systems were described in terms of the covalent exchange of neutrons between the α -cores. Again the building blocks are the α -particles and the neutrons are shared between the cores. This is highly reminiscent of the exchange of electrons in covalently bound atomic molecules. For example, the H_2^+ molecule is formed from two protons with a covalently exchanged electron. The electrons reside in single center s -orbitals and the covalent bond is formed from their linear combination:

$$\psi_{\pm} = \frac{1}{\sqrt{2}}(\varphi_1 \pm \varphi_2). \quad (1.20)$$

This generates two molecular wave-functions, one with no intermediate node (bonding) and a higher energy state with an internal node (anti-bonding). The development of atomic orbitals from symmetry adapted linear combinations (SALCs), is also widely used in molecular physics.

The exchange of neutrons between α -particle cores is a rather important concept which allows a detailed understanding of the structure of the beryllium isotopes to be developed [85–89]. The appearance of nuclear molecules is reviewed in [6]. The nucleus ${}^9\text{Be}$ demonstrates this beautiful piece of physics rather well. The $N = Z$ isotope ${}^8\text{Be}$ is unstable against α -decay, held together only by the Coulomb barrier for a period of $\sim 10^{-16}$ seconds. The only stable beryllium isotope is ${}^9\text{Be}$. The additional neutron is exchanged between the cores just as electrons are exchanged between atoms in covalent atomic molecules. Thus, such states have been coined *nuclear molecules*. It is the delocalisation of the neutron which lowers its kinetic energy giving an enhanced binding energy for the ${}^9\text{Be}$ system compared to ${}^8\text{Be}$. It is inferred from the neutron separation energy in ${}^9\text{Be}$ that the magnitude of the binding is approximately 1.6 MeV [86].

In the formation of such molecular states in the beryllium isotopes, the single-center wave-functions are those that the neutrons occupy in ${}^{5,6}\text{He}$, i.e. $p_{3/2}$. Thus, one might expect the neutron to reside in covalent orbits, which are the analogues

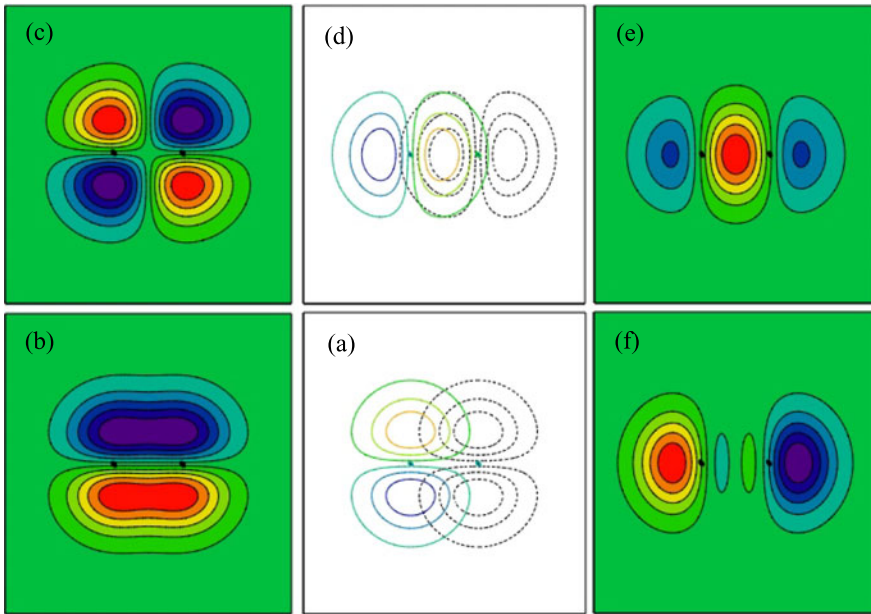


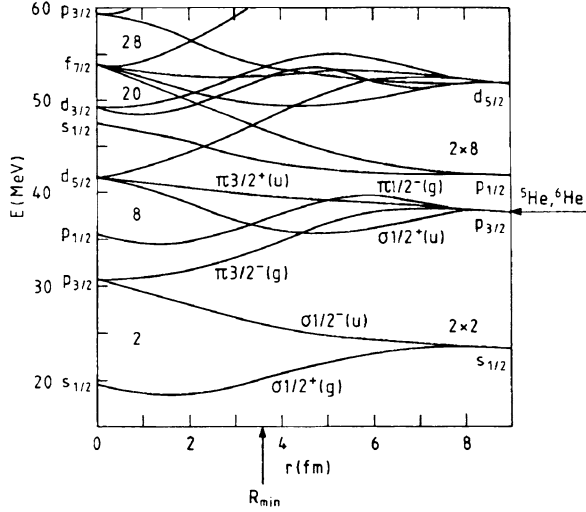
Fig. 1.20 Molecular orbitals associated with linear combinations of HO orbitals $[n_{\perp}, n_z] = [1, 0]$ and $[0, 1]$ orbits, equivalent to p -states. Here the z -direction is aligned with the separation axis of the two centers indicated by the *black dots*. (a) Shows the overlap of the two individual wavefunctions. Diagrams (b) and (c) are the result of forming linear combinations: (b) corresponds to the binding π -state, and (c) to the anti-binding state. Diagram (d) shows the overlap of the two $(0, 0, 1)$ orbits, forming the σ -configurations, and (e) and (f) the two linear combinations

of those observed in carbon and oxygen molecules, namely σ and π -orbitals, which are formed in the exchange of p -electrons.

To illustrate this, the possible linear combinations of the equivalent HO orbitals $[n_{\perp}, n_z] = [1, 0]$ and $[0, 1]$ are shown in Fig. 1.20. Note that there are two possible orientations of the dumbbell-like orbitals—either parallel or perpendicular to the axis separating the α -particles (though phases may vary). The linear combination shown in part (b) corresponds to the π -type structure for the valence neutron, and (e) to the σ -orbital. The notation σ and π corresponds to the projection of the angular momentum of the molecular orbit onto the symmetry axis of the molecule. If the linear combination of the p -orbitals is considered, then for the orientation shown in Fig. 1.20a, this would correspond to $l = 1$ components along the separation axis and hence π -type orbitals. For the alternate case, Fig. 1.20d, the projection of the orbital angular momentum of the two p -orbitals is perpendicular to the separation axis and thus the σ association (no angular momentum).

Figure 1.21 shows the energy evolution of the energy levels of the two-center shell model, where the Schrödinger equation is solved for two shell model potentials as a function of their separation—from infinite separation to zero. This model is one which is appropriate for the description of the merger of two nuclei (with

Fig. 1.21 The energy levels of the two center shell model from [87, 88]. The separation of the two potentials is defined in terms of the distance r . The present calculation corresponds to the energy-levels associated with the fusion of two ${}^4\text{He}$ nuclei. The separation at which the interaction potential reaches a minimum, R_{\min} —this would correspond to the ${}^8\text{Be}$ ground state



zero impact parameter forming a composite system) and traces the evolution of the initially degenerate energy levels in the two separate potentials to those of the merged system. As the separation varies, then the energy levels are essentially those of the prolate deformed nucleus and will strongly overlap with those found in the deformed shell, Nilsson, model (as illustrated in Fig. 1.22). The separation of the two potentials appropriate for two α -particles in the ground state of ${}^8\text{Be}$ is marked $R_{\min} \sim 3.5$ fm in Fig. 1.21—the point at which the α - α potential attains its minimum. At this separation the two lowest energy orbits available for the neutron to follow are marked $\pi 3/2^-$ and $\sigma 1/2^+$. In fact the two levels are almost degenerate. These two orbits are analogues of the Nilsson orbitals from the $1p_{3/2}$ and $1d_{5/2}$ levels, with projections of the total angular momentum $K^\pi = 3/2^-$ and $1/2^+$, respectively.

A natural conclusion is that if such a description of ${}^9\text{Be}$ is correct then the ground state of ${}^9\text{Be}$ should be the head of a rotational band associated with $K^\pi = 3/2^-$. There should also be a second band linked with a $K^\pi = 1/2^+$ configuration and both bands should have a similar rotational gradient as that of the ${}^8\text{Be}$ ground state. In fact one would expect the $K^\pi = 1/2^+$ band to be slightly more deformed than the ground state band as the valence neutron in the σ -configuration intercedes between the two α -particles enhancing the deformation. Figure 1.23 shows the experimental situation for the nuclei ${}^8\text{Be}$, ${}^9\text{Be}$ and ${}^{10}\text{Be}$. The data indeed confirms the prediction; aside from the fact that the $K = 1/2$ band possesses Coriolis decoupling. For such bands, an additional term is introduced with an associated Coriolis decoupling parameter a ,

$$E_J = \frac{\hbar^2}{2\mathcal{I}} [J(J+1) + (-)^{J+1/2} a(J+1/2)] \quad (1.21)$$

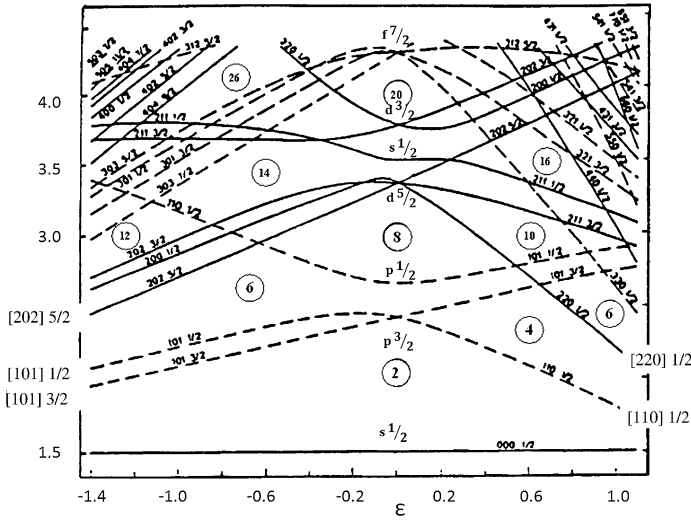


Fig. 1.22 The Nilsson single-particle energy levels. The parameter ϵ corresponds to the deformation of the potential. The magic numbers are labelled as are some of the key Nilsson orbits [90]

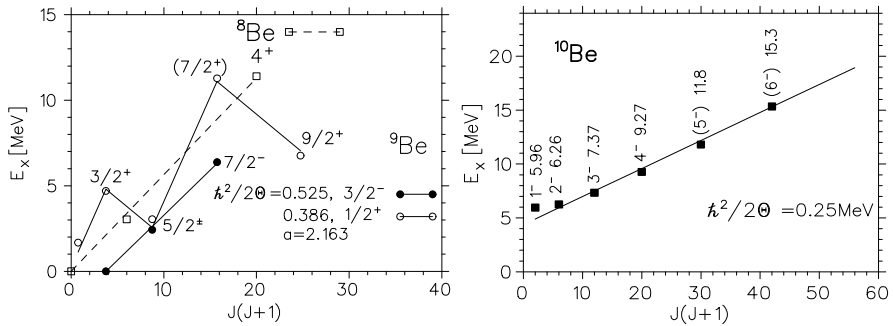


Fig. 1.23 Rotational bands of ^8Be , ^9Be (left side) and ^{10}Be (right side). The excitation energies are plotted as a function of angular momentum $J(J + 1)$. The Coriolis decoupling parameter, α , for the $K = 1/2$ band is indicated. From Ref. [91]

\mathcal{I} being the moment of inertia. It should be noted that the experimental moment of inertia for the $K = 1/2$ band is indeed larger than for the $K = 3/2$ ground-state band (as indicated in the left hand part of the figure).

1.7.1 The Neutron-Rich Nucleus ^{10}Be

The addition of two neutrons to the two α -particles results in the formation of ^{10}Be . The AMD calculations for the nucleus are shown in Fig. 1.24 [92]. The contour

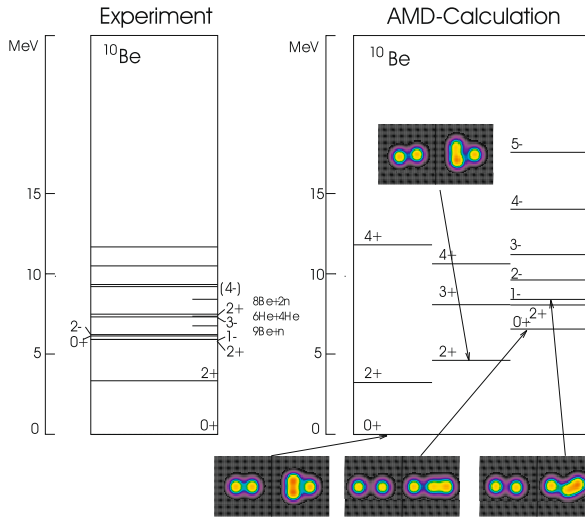


Fig. 1.24 *Left side:* Experimental level scheme of ^{10}Be , and, *right side:* that calculated with the spin parity projected AMD model [92]. The density plots of the intrinsic states are shown in special panels: for protons on the *left side* of each plot and for neutrons on the *right side*, respectively. The proton densities represent the positions of the α -particles. The neutron densities show for the ground state a density distribution characteristic of π -binding. The higher lying $0^+ 2^+$ state is well reproduced with a larger α - α distance (seen by the density of protons) as compared to the ground state, it shows the σ^2 configuration for the neutrons. The density of the 1^- state shows a mixture of σ - π orbitals with a distorted neutron density

plots show the density of the protons (left side) and neutrons (right side). In the case of the protons the α -particle structure can be clearly be seen. In the first 0^+ state (ground-state) the separation of the “ α -particles” is smaller than that corresponding to the next 0^+ state ($0^+ 2^+$). In the molecular picture this can be understood in terms of the orbitals of the valence neutrons. In the ground-state the neutrons occupy the π -orbital, forming a bridge between the two centers, whilst for the second 0^+ state the neutrons intercede between the two α -particles in a σ -orbital. The effect of the Pauli Exclusion Principle is to make it energetically unfavorable for the valence neutrons and those in the α -particle to overlap and hence the two α -particles are forced apart in order to minimize the energy of the configuration.

The $0^+ 2^+$ state should thus be the more deformed of the two—in fact could be the most deformed nuclear state yet seen in nature—experimentally it is found at 6.1793 MeV. The gamma-decay of this state is suppressed (it possesses a lifetime of the order of 1 ps)—an isomeric behavior that may be understood in terms of the small overlap of its structure and that of the more compact ground state. The excited state at 7.542 MeV (2^+) is believed the first rotational member of the associated band. This state lies very close to the α -decay threshold (7.409 MeV) and thus its decay to this channel is strongly suppressed by the Coulomb and ($L = 2$) centrifugal barriers. Nevertheless, the α -decay has been found to correspond to a very large reduced width [93], representative of the large degree of clusterisation associated

with the state. This is however a single, and very challenging, measurement and needs confirming.

The 4^+ member of the same band would lie in the region of 10–11 MeV. There are a number of possible states which could correspond to the molecular band; 10.15 MeV and 10.57 MeV. The spin of the latter state is unknown, whereas the former has been associated with spins 3^- [94] and 4^+ [95]. The latter assignment was also found in a measurement of the resonant scattering of ${}^6\text{He}+{}^4\text{He}$ [96]. Recent re-measurements of resonant scattering verify the 4^+ assignment [97]. The energy and width of the state are consistent with the interpretation of an extremely deformed rotational band with a well-developed cluster structure.

Determination of the structure the ground-state of ${}^{10}\text{Be}$ cannot be readily made using particle spectroscopy techniques. A recent set of measurements of the electromagnetic transition strengths, $B(E2)$, between the 2^+ and 0^+ ground-state for ${}^{10}\text{Be}$ and ${}^{10}\text{C}$, together with the isobaric analogue state in ${}^{10}\text{B}$ [98, 99] (made with an unprecedented precision) provide a significant benchmark against which the character of the state may be fixed.

The observations made for the nuclei ${}^9\text{Be}$ and ${}^{10}\text{B}$ may be extended to more complex $2\alpha+Xn$ systems such as ${}^{11,12}\text{Be}$ where the valence neutrons can be thought of as occupying combinations of σ and π -orbitals. The interactions between these valence particles will perturb the zeroth order molecular picture, but it is understood that some of the molecular characteristics are retained [6].

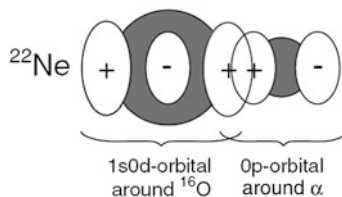
1.7.2 More Complex Molecular States and the Extended Ikeda Diagram

1.7.2.1 Asymmetric Cores

Based upon the concept that neutrons may be exchanged between α -particles it has been proposed that it may also be possible to form covalent structures from non- α cores in other systems. The next best two centered case corresponds to cores formed from an α -particle and an ${}^{16}\text{O}$ nucleus. ${}^{16}\text{O}$ possesses a closed shell, but not quite the degree of inertness of the α -particle (it has a first excited state of 6.05 MeV, 0^+ , compared with 20.2 MeV). Nuclei formed from these two components produce neon isotopes. The nucleus ${}^{20}\text{Ne}$ is known to have a well-developed $\alpha+{}^{16}\text{O}$ cluster structure [55, 100, 101], the asymmetric structure giving rise to two rotational bands of $K^\pi = 0^\pm$ character [102]. The question as to what happens to valence neutrons introduced into this system was addressed by von Oertzen [103]. When the neutron orbits the α -particle it lies in a p -orbital (negative parity), when orbiting the closed shell ${}^{16}\text{O}$ it resides in the sd -shell (positive parity, associated with the $5/2^+$ ground-state).

The two orbitals which are aligned with the intrinsic deformation of the α - ${}^{16}\text{O}$ system are linked to the harmonic oscillator levels $[n_x, n_y, n_z] = [0, 0, 1]$ and $[0, 0, 2]$. These are associated with the Nilsson orbitals with projections $K^\pi = 1/2^-$

Fig. 1.25 The covalent exchange of a neutron between the ^{16}O and α cores that occurs in the neon isotopes, from Ref. [104]



and $1/2^+$; both have σ -character. The strong overlap of these two orbitals in the region between the cores gives rise to the molecular binding effect, illustrated in Fig. 1.25. The resulting hybridized orbital gives rise to parity doublet bands [103]. For a complete description of the molecular bands that appear in the neutron-rich isotopes see Ref. [6].

1.7.2.2 More than Two Centers

The obvious extension from $2\alpha + Xn$ systems is to nuclei composed of 3α -particles—carbon isotopes. In this instance the α -particle cores may adopt a number of different arrangements. Two possible limits are a triangular and linear arrangements. This creates a greater spectrum of molecular states and hence complexity. There are a number of theoretical predictions for the appearance and characteristics of such states [6, 105, 106]. From the experimental perspective there is no definitive evidence for their existence [6], though measurements of ^{13}C and ^{14}C indicate possible rotational bands with the right characteristics.

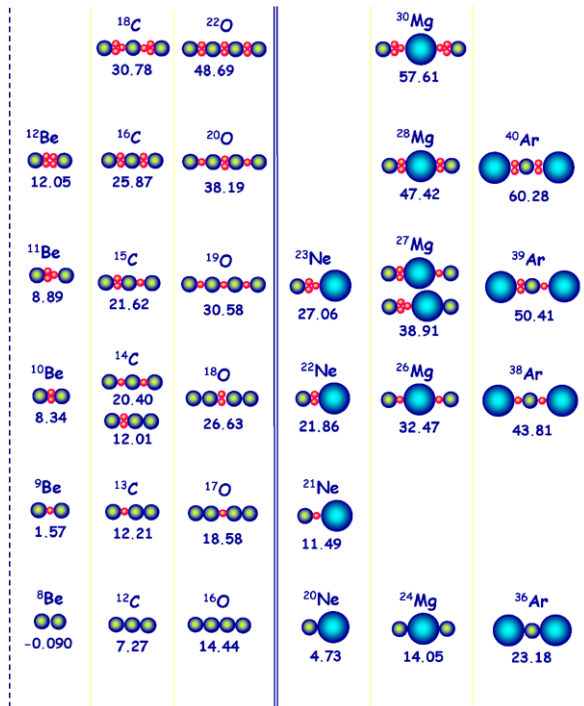
1.7.2.3 The Extended Ikeda Diagram

The possibility that beyond α -conjugate nuclei there exists a series of states whose properties are strongly influenced by the underlying α -particle cluster structure, where the valence particles have the imprint of molecular exchange of the valence particles opens up some exciting possibilities. The present state-of-play is that only a few of these possibilities have been characterized. Understanding the conditions under which these states might appear is important and one element is the threshold energy—in most cases the states will not be close to the ground-state. Motivated by the Ikeda Diagram for α -conjugate cases (Fig. 1.5) von Oertzen has devised an *extended Ikeda Diagram* which is shown in Fig. 1.26. The diagram charts the expected location of these exotic states in terms of the constituent particle decay thresholds.

There are a number of intriguing possibilities in terms of new structures, for example the evolution of the behavior of the Beryllium isotopes ^8Be to ^{12}Be with increasing numbers of neutrons is indicated, as is the evolution of the 3α -systems.

Perhaps the one that captures the imagination most is that characterized by the structure $\alpha + 2n + ^{16}\text{O} + 2n + \alpha$, in ^{28}Mg . This state has been called *nuclear water* due to the similarity with the atomic H_2O , however due to the nature of the valence orbitals it more closely resembles CO_2 . Identification of such a structure would be an experimental tour-de-force.

Fig. 1.26 The modified Ikeda Diagram proposed by von Oertzen. The *left hand side* shows the case for structures composed of α -particles (blue) and neutrons (red). The *right hand side* shows the case for larger cores of ^{16}O nuclei (larger blue spheres). The numbers shown are the excitation energies at which the cluster structures are expected to appear and correspond to the cluster binding energies



1.8 Summary and Conclusions

The history of clustering reaches to the earliest days of nuclear science when some of the first models captured nuclear properties in terms of constituent α -particles. Though the initial pictures have been found to be overly simplistic there are a number of cases where nuclei appear to have a behavior which reflects a well-developed α -particle structure. Key examples of these states are the ^8Be ground-state and the 7.65 MeV, 0^+ , Hoyle-state in ^{12}C . It is nuclei such as this which have become the touchstones for the development of state-of-the-art nuclear models. Much of nuclear science has moved from this territory to the drip-lines—the limits of isospin stability. It is here that there is a significant increase in the number of neutrons, for example. It is in such systems that there is a co-existence of the boson and fermionic degrees of freedom and the valence neutrons can be thought of as being covalently exchanged between the α -particle cores. Though systems such as ^9Be and ^{10}Be are well characterized in these terms, the precise influence at the drip-lines has yet to be established. There is no doubt that correlations at the drip-lines play a defining role, but the question for the future is if they precipitate clusterization.

Acknowledgements The author would like to acknowledge his many colleagues who have worked on the development of both experimental and theoretical ideas contained in this review.

References

1. R.B. Wiringa, S.C. Pieper, J. Carlson, V.R. Pandharipande, *Phys. Rev. C* **62**, 014001 (2000)
2. J. Fujita, H. Miyazawa, *Prog. Theor. Phys.* **17**, 360 (1957)
3. L.R. Hafstad, E. Teller, *Phys. Rev.* **54**, 681 (1938)
4. H. Morinaga, *Phys. Rev.* **101**, 254 (1956)
5. K. Ikeda, N. Tagikawa, H. Horiuchi, *Prog. Theor. Phys. Suppl.*, extra number, 464 (1968)
6. W. von Oertzen, M. Freer, Y. Kanada En'yo, *Phys. Rep.* **432**, 43 (2006)
7. N. Itagaki, W. von Oertzen, S. Okabe, *Phys. Rev. C* **74**, 067304 (2006)
8. A. Bohr, B.R. Mottelson, *Nuclear Structure*, vol. II (Benjamin, Reading, 1975)
9. M. Freer, R.R. Betts, A.H. Wuosmaa, *Nucl. Phys. A* **587**, 36 (1995)
10. W. Nazarewicz, J. Dobaczewski, *Phys. Rev. Lett.* **68**, 154 (1992)
11. T. Bengtsson, M.E. Faber, G. Leander, P. Moller, M. Ploszajczak, I. Ragnarsson, S. Aberg, *Phys. Scr.* **24**, 200 (1981)
12. W.D.M. Rae, *Int. J. Mod. Phys.* **3**, 1343 (1988)
13. N. Itagaki, S. Aoyama, S. Okabe, K. Ikeda, *Phys. Rev. C* **70**, 054307 (2004)
14. N. Itagaki, H. Masui, M. Ito, S. Aoyama, *Phys. Rev. C* **71**, 064307 (2005)
15. H. Masui, N. Itagaki, *Phys. Rev. C* **75**, 054309 (2007)
16. R.E. Peierls, J. Yoccoz, *Proc. Phys. Soc. Lond. A* **70**, 381 (1957)
17. J.M. Blatt, *Austr. Math. Soc.* **1**, 465 (1960)
18. H. Margenau, *Phys. Rev. C* **59**, 37 (1941)
19. D.M. Brink, in *Proceedings of the International School of Physics "Enrico Fermi", Course 36*, Varenna, 1965, ed. by C. Bloch (Academic Press, New York, 1966), p. 247
20. W. Bauhoff, H. Schultheis, R. Schultheis, *Phys. Rev. C* **29**, 1046 (1984)
21. S. Marsh, W.D.M. Rae, *Phys. Lett. B* **180**, 185 (1986)
22. A.C. Merchant, W.D.M. Rae, *Nucl. Phys. A* **549**, 431 (1992)
23. J. Zhang, W.D.M. Rae, *Nucl. Phys. A* **564**, 252 (1993)
24. J. Zhang, W.M.D. Rae, A.C. Merchant, *Nucl. Phys. A* **575**, 61 (1994)
25. A. Tohsaki et al., *Phys. Rev. Lett.* **87**, 192501 (2001)
26. Y. Funaki, A. Tohsaki, H. Horiuchi, P. Schuck, G. Röpke, *Phys. Rev. C* **67**, 051306 (2003)
27. T. Yamada, P. Schuck, *Phys. Rev. C* **69**, 024309 (2004)
28. G. Röpke, P. Schuck, *Mod. Phys. Lett. A* **21**, 2513 (2006)
29. Y. Funaki, A. Tohsaki, H. Horiuchi, P. Schuck, G. Röpke, *Eur. Phys. J. A* **28**, 259 (2006)
30. I. Sick, J.S. McCarthy, *Nucl. Phys. A* **150**, 631 (1970)
31. A. Nakada, Y. Torizuka, Y. Horikawa, *Phys. Rev. Lett.* **27**, 745 (1971) and 1102 (Erratum)
32. P. Strehl, Th.H. Schucan, *Phys. Lett. B* **27**, 641 (1968)
33. J.A. Wheeler, *Phys. Rev.* **52**, 1083 and 1107 (1937)
34. D.L. Hill, J.A. Wheeler, *Phys. Rev.* **89**, 1102 (1953)
35. J.J. Griffin, J.A. Wheeler, *Phys. Rev.* **108**, 311 (1957)
36. K. Wildermuth, W. McClure, in *Cluster Representations of Nuclei*. Springer Tracts in Modern Physics, vol. 41 (Springer, Berlin, 1966)
37. K. Wildermuth, Y.C. Tang, in *A Unified Theory of the Nucleus* (Academic Press, New York, 1977)
38. A. Arima, H. Horiuchi, K. Kubodera, N. Takigawa, *Adv. Nucl. Phys.* **5**, 345 (1972) (Plenum, New York, 1972). Edited by Baranger M. and Vogt E.
39. H. Furutani, H. Kanada, T. Kaneko, S. Nagata, H. Nishioka, S. Okabe, S. Saito, T. Sakuda, M. Seya, *Prog. Theor. Phys. Suppl.* **68**, 193 (1980)
40. Y.C. Tang, M. LeMere, D.R. Thompson, *Phys. Rep.* **47**, 167 (1978)
41. K. Langanke, H. Friedrich, *Adv. Nucl. Phys.* **17**, 223 (1987) (Plenum, New York, 1987). Edited by Negele J.W. and Vogt E.
42. K. Langanke, *Adv. Nucl. Phys.* **21**, 85 (1994) (Plenum, New York, 1994). Edited by Negele J.W. and Vogt E.
43. D. Baye, P.-H. Heenen, *Nucl. Phys. A* **233**, 304 (1974)
44. D. Baye, P.-H. Heenen, M. Liebert-Heinemann, *Nucl. Phys. A* **291**, 230 (1977)

45. D. Baye, P. Descouvemont, in *Proceedings of the fifth International Conference on "Clustering aspects in nuclear and subnuclear systems"*, Kyoto, Japan, 25th–29th July ed. by K. Ikeda, K. Katori, Y. Suzuki (1988), p. 103 [Supplement to the Journal of the Physical Society of Japan, vol. 58 (1989)]
46. D. Baye, in *Proceedings of the Sixth International Conference on "Clusters in Nuclear Structure and Dynamics"*, Strasbourg, France, 6th–9th September 1994, ed. by F. Haas (1994), p. 259
47. P. Descouvemont, Nucl. Phys. A **699**, 463 (2002)
48. N. Itagaki, S. Hirose, T. Otsuka, S. Okabe, K. Ikeda, Phys. Rev. C **65**, 044302 (2002)
49. N. Itagaki, S. Okabe, Phys. Rev. C **61**, 044306 (2000)
50. N. Itagaki, S. Okabe, K. Ikeda, Phys. Rev. C **62**, 034301 (2000)
51. N. Itagaki et al., Phys. Rev. C **64**, 014301 (2001)
52. M. Ito, Phys. Lett. B **636**, 293 (2006)
53. L.D. Landau, E.M. Lifshitz, *Quantum Mechanics*, 3rd edn. (Elsevier, Butterworth–Heinemann, Amsterdam/Stoneham, 1958)
54. H. Nakamura, *Nonadiabatic Transition* (World Scientific, Singapore, 2000) and references therein
55. Y. Kanada-En'yo, H. Horiuchi, Prog. Theor. Phys. **142**, 205 (2001)
56. R. Roth, T. Neff, H. Hergert, H. Feldmeier, Nucl. Phys. A **745**, 3 (2004)
57. M. Chernykh, H. Feldmeier, T. Neff, von P. Neumann-Cosel, A. Richter, Phys. Rev. Lett. **98**, 032501 (2007)
58. P. Navrátil et al., J. Phys. G **36**, 083101 (2009)
59. E. Epelbaum, Part. Nucl. Phys. **57**, 654 (2006)
60. E. Epelbaum, H.-W. Hammer, U.-G. Meißner, Rev. Mod. Phys. **81**, 1773 (2009)
61. P. Navrátil, J.P. Vary, B.R. Barrett, Phys. Rev. Lett. **84**, 5728 (2000)
62. P. Navrátil, V. Gueorguiev, J.P. Vary, W.E. Ormand, A. Nogga, Phys. Rev. Lett. **99**, 042501 (2007)
63. E. Epelbaum, H. Krebs, T.A. Lähde, D. Lee, U.-G. Meißner, Phys. Rev. Lett. **110**, 112502 (2013)
64. E. Epelbaum, H. Krebs, T.A. Lähde, D. Lee, U.-G. Meißner, Phys. Rev. Lett. **109**, 252501 (2012)
65. E. Epelbaum, H. Krebs, D. Lee, U.-G. Meißner, Phys. Rev. Lett. **106**, 192501 (2011)
66. R. Bijker, F. Iachello, Phys. Rev. C **61**, 067305 (2000)
67. M. Freer et al., Phys. Rev. C **76**, 034320 (2007)
68. F. Hoyle, Astrophys. J. Suppl. Ser. **1**, 12 (1954)
69. C.W. Cook et al., Phys. Rev. **107**, 508 (1957)
70. G.M. Reynolds, D.E. Rundquist, M. Poichar, Phys. Rev. C **3**, 442 (1971)
71. F.D. Smit et al., Phys. Rev. C **86**, 03701 (2012)
72. M. Itoh et al., Nucl. Phys. A **738**, 268 (2004)
73. M. Itoh et al., Phys. Rev. C **84**, 054308 (2011)
74. M. Freer et al., Phys. Rev. C **86**, 034320 (2012)
75. M. Freer et al., Phys. Rev. C **80**, 041303(R) (2009)
76. W.R. Zimmerman, N.E. Destefano, M. Freer, M. Gai, F.D. Smit, Phys. Rev. C **84**, 027304 (2011)
77. W.R. Zimmerman et al., Phys. Rev. Lett. **110**, 152502 (2013)
78. M. Freer et al., Phys. Rev. C **83**, 034314 (2011)
79. K.P. Artemov et al., Sov. J. Nucl. Phys. **52**, 406 (1990)
80. G.V. Rogachev et al., Phys. Rev. C **64**, 051302 (2001)
81. M. Freer, A.C. Merchant, J. Phys. G **23**, 261 (1997)
82. M. Freer, Nucl. Instrum. Methods A **383**, 463 (1996)
83. P.J. Haigh, Phys. Rev. C **79**, 014302 (2009)
84. S. Aoyama, S. Mukai Kato, K. Ikeda, Prog. Theor. Phys. **93**, 99 (1995)
85. M. Seya, M. Kohno, S. Nagata, Prog. Theor. Phys. **65**, 204 (1981)
86. W. von Oertzen, Z. Phys. A **354**, 37 (1996)

87. W. von Oertzen, *Z. Phys. A* **357**, 355 (1997)
88. W. von Oertzen, *Nuovo Cimento A* **110**, 895 (1997)
89. N. Itagaki, S. Okabe, *Phys. Rev. C* **61**, 044306 (2000)
90. S.G. Nilsson, *Mat. Fys. Medd. Dan. Vid. Selsk.* **29**, 16 (1955)
91. H.G. Bohlen, W. von Oertzen, A. Blazevic, B. Gebauer, M. Milin, T. Kokalova, Ch. Schulz, S. Thummerer, A. Tumino, in *Proceedings of the International Symposium on Exotic Nuclei, Lake Baikal, Russia, 2001*, ed. by Yu.E. Penionzhkevich, E.A. Cherepanov (World Scientific, Singapore, 2002), p. 453
92. Y. Kanada-En'yo, H. Horiuchi, A. Dóte, *J. Phys. G* **24**, 1499 (1998)
93. J.A. Liendo et al., *Phys. Rev. C* **65**, 034317 (2002)
94. N. Curtis et al., *Phys. Rev. C* **64**, 044604 (2001)
95. M. Milin et al., *Nucl. Phys. A* **753**, 263 (2005)
96. M. Freer et al., *Phys. Rev. Lett.* **96**, 042501 (2006)
97. G. Rogachev, (2012), Private communication
98. E.A. McCutchan et al., *Phys. Rev. C* **86**, 057306 (2012)
99. E.A. McCutchan et al., *Phys. Rev. C* **86**, 014312 (2012)
100. H. Horiuchi, K. Ikeda, *Prog. Theor. Phys. A* **40**, 277 (1968)
101. Y. Kanada En'yo, H. Horiuchi, *Prog. Theor. Phys.* **93**, 115 (1995)
102. P.A. Butler, W. Nazarewicz, *Rev. Mod. Phys.* **68**, 350 (1996)
103. W. von Oertzen, *Eur. Phys. J. A* **11**, 403 (2001)
104. M. Kimura, *Phys. Rev. C* **75**, 034312 (2007)
105. P. McEwan, M. Freer, *J. Phys. G* **30**, 1 (2004)
106. N. Itagaki, T. Otsuka, K. Ikeda, S. Okabe, *Phys. Rev. Lett.* **92**, 014301 (2004)